JOURNAL OF GEOPHYSICAL RESEARCH, VOL. 89, NO. B7, PAGES 5771-5790, JULY 10, 1984

Modification of Wave-Cut and Faulting-Controlled Landforms

THOMAS C. HANKS, ROBERT C. BUCKNAM, KENNETH R. LAJOIE, AND ROBERT E. WALLACE

U. S. Geological Survey

From a casual observation that the form of degraded fault scarps resembles the error function, this investigation proceeds through an elementary diffusion equation representation of landform evolution to the application of the resulting equations to the modern topography of scarplike landforms. The morphologic observations can be analyzed either in the form of one or more cross-strike elevation profiles or in the form of the slope-offset plot, a point plot of maximum scarp slope versus scarp offset. Working with either or both of these data representations for nine geologic structures, which range in age from 3 to 400 ka B.P. and in offset from 1 to 50 m, we apply analytical solutions for the vertical initial value scarp, the vertical continuous offset scarp, and the finite slope, initial value scarp. The model calculations are intrinsically ambiguous, yielding as the final answer only the product κt (in the case of the initial value problem) or the product κA^{-1} (in the case of the repeated faulting problem); here t is the age of a single scarp-forming event, $2A$ is the vertical slip rate, and κ is the "mass diffusivity." A single profile across three sea cliffs along the Santa Cruz, California, coast is analyzed as three separate initial value problems. A reasonably constrained age for the sea cliff standing above the Highway 1 platform returns $\kappa = 11$ GKG (1 GKG = 1 m^2/ka). With this κ, we can date the two older sea cliffs. In fact, we do the converse: age estimates for these two older sea cliffs based on a uniform rate of uplift both yield the same κ as for the lower sea cliff. We treat a single profile of the Raymond fault in Pasadena/San Marino in terms of the repeated faulting problem; for it the uplift rate of R. Crook and others yields $\kappa = 16$ GKG. The very substantial preexisting offset across the Raymond fault must have been buried/leveled some 230 ka B.P., when the modern topography began to form. Our analysis of the Lake Bonneville shoreline scarps reveals a dependence of κt on $2a$, suggestive of nonlinear modification processes. This appearance is treated with the finite slope initial value scarp model to determine $\kappa = 1.1$ GKG for the Lake Bonneville shoreline scarps. The suggestion of M. N. Machette that approximately 100,000-year-old, meter-high scarps are "unobservable" in weakly consolidated alluvial terranes of the Basin and Range and Rio Grande Rift Valley provinces can be formulated as $\kappa \gtrsim 1$ GKG. The coincidence between this inequality and the Lake Bonneville shoreline κ is striking, and it suggests that the value of $\kappa = 1$ GKG may be generally applicable, as a good first approximation, to the modification of alluvial terranes within the semiarid regions of the western United States. The Lake Bonneville shoreline κ is the basis for dating four sets of fault scarps in west-central Utah. The Drum Mountains fault scarps can be modeled in several different circumstances, but the most likely interpretation is that these fault scarps formed as the result of a single episode of normal faulting 3.6 to 5.7 ka B.P. The younger age is associated with quite low initial slope angles (25°). The other three sets of fault scarps show no evidence for finite initial value slopes. Fault scarps along the eastern base of the Fish Springs Range are very young, 3 ka B.P. We estimate the age of fault scarps along the western flank of the Oquirrh Mountains to be 32 ka B.P., which meets the weak geologic constraint that they be older than the Lake Bonneville shoreline. Fault scarps along the northeastern margin of the Sheeprock Mountains are even older, 53 ka B.P. An intriguing consequence of our single-event analysis of these scarps is that an 11.5-m offset occurred in a single earthquake.

INTRODUCTION

The processes and rates of landform evolution have long intrigued students of earth history, but such matters have not yielded easily to quantitative analysis. In the first place, a myriad of processes contribute to landform modification, and these can take any number of physical, chemical, biological, and, nowadays, cultural forms. Second, many if not all of these processes must depend on the considerable range of environmental variables that the earth provides, in the form of different climates and geologic materials, for example. Finally, landform evolution implies morphologic changes with time, but only rarely is anything but the present-day configuration available for study.

Given such difficulties, a study such as this, which intends to analyze scarplike landforms using a highly idealized model of erosional evolution, would not seem to hold much promise; that it exists at all is due to three related but distinct circumstances, one of them essentially fortuitous. The first of these is the compelling need for more accurate and precise estimates of earthquake recurrence intervals. For most seismogenic areas of the world the principal uncertainity in earthquake risk analysis is the uncertainty in recurrence intervals of potentially damaging or destructive earthquakes. On the outcome of such calculations (and their attendant uncertainties) ride enormous sums of human and financial commitments. For most of these areas, however, the only available record of major earthquakes of the past exists in geologic manifestations of faulting. Detailed mapping of active crustal faults sectioned by trenches has often proved fruitful in dating one or more ancient faulting episodes [e.g., *Clark et al.*, 1972; *Sieh*, 1978], but such investigations are expensive, time consuming, and often as not dependent on special circumstances that allow the site to be simultaneously preserved but exposed.

Much information concerning ancient faulting episodes and recurrence intervals, however, exists in more readily obtainable observations of the morphology of presently existing fault scarps. Although the detailed geomorphology of Holocene and late Pleistocene fault scarps is a relatively new field [e.g., *Wallace*, 1977; *Bucknam and Anderson*, 1979], there is now ample evidence that fault scarps in different states of degradation surely reflect different dates of formation [e.g., *Wallace*, 1977, Figure 3; *Bucknam and Anderson*, 1979, Figure 5], the

Paper number 4B0164.

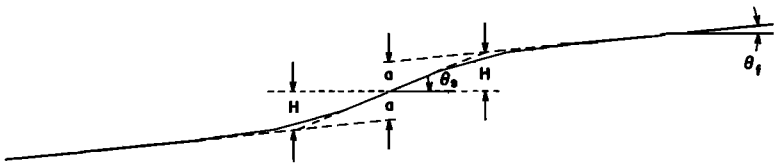

Fig. 1. The geometry of a fault scarp, mostly after *Bucknam and Anderson* [1979]. In this study, we refer to $2a$ as the scarp offset and $2H$ as the scarp height. In the presence of nonzero θ_f, these amplitude measurements are not the same (see equation (11)); θ_s and θ_f are, respectively, the scarp slope angle and the far-field slope angle; the tangents of these angles are the scarp slope $\partial u/\partial x|_{x=0}$ and the far-field slope b, respectively.

potential difficulties detailed two paragraphs above notwithstanding.

Finally, it has been our casual observation that the form of degraded fault scarps resembles the error function; the error function, in turn, forms the fundamental solution to the one-dimensional diffusion equation for steplike initial conditions (for example, a newly formed fault scarp). The fulcrum of this investigtion, then, is the notion that the difffusion equation is a simple and believable first-order mathematical approximation to the erosional evolution of nondissecting alluvial terranes. That this seems to be the case is the reason we continue at all.

We develop and rationalize the diffusion equation representation in the next section and discuss in some detail there the solutions appropriate for the problems of interest in this investigation, but a few general remarks concerning its nature and earlier use in geomorphology are appropriate here. Given the purposes of this study, our preference for the diffusion equation model is not only that it can be obtained with elementary and believable assumptions but that it seems to make sense, within limits, for the nine geologic structures analyzed here. Moreover, the general and macroscopic nature of the diffusion equation allows one to know not a thing about any specific erosional process; all such effects materialize in a single parameter κ, the topographic equivalent of the thermal diffusivity. To the extent that this equation is valid, then, we may study landform modification in much the same way as heat conduction was understood in the nineteenth century. In the absence of an atomic theory of solids and temperature, one did not know the physical mechanisms by which heat transport actually took place; one just knew that it did, given a temperature gradient. This study proceeds on the same basis: there is no statement herein about the mechanisms by which mass transport takes place, leading to landform modification; we simply assume that it does, given a topographic gradient, and parameterize all such mechanisms with κ, here referred to as the mass diffusivity. Nevertheless, we proceed on less sure physical grounds: the diffusion equation representation of heat conduction is directly verifiable, whereas our model of nonsteady scarp evolution is not. The essence of this investigation, then, is not whether the diffusion equation representation of landform evolution is correct, in terms of whatever entirety of "first principles" is appropriate, but whether or not this description works, in the sense of explaining geomorphologic observations.

The diffusion equation representation of landform modification is not new to geomorphology, and G. K. Gilbert in his field notes of October 27, 1876, contemplated the connection between erosional rounding of badland crests and heat conduction into wedge-shaped bodies (A. M. Johnson and D. D. Pollard, unpublished manuscript, 1977, p.71). Even so, *Culling* [1960] seems to have been the first to propose this model explicitly and to lay out its underlying assumptions; he noted, in particular, the error function solutions arising from initial conditions appropriate for faulting. *Culling* [1963, 1965] attributed the basic processes underlying the diffusion equation representation to stochastic properties of soil creep. *Hirano* [1968] discussed the applicability of more general, diffusionlike equations to various problems in geomorphology and compiled a large number of solutions for them.

Very little work, however, has been done to verify the theoretical postulates of Culling and Hirano, that is, to apply the diffusion equation representation to real geomorphologic data. *Hirano* [1969] used his earlier results to investigate the long-term topography, uplift rate, and recessional velocity of the Yoro Mountains, central Japan. *Soderblom* [1970] developed a diffusion equation representation of lunar crater evolution in the presence of impact modification to analyze their observed size distribution characteristics. *Nash* [1980*a*] utilized the diffusion equation framework to analyze two sets of Holocene shoreline scarps of different ages in Emmet County, Michigan. Only *Nash* [1980*b*], however, seems to have brought this approach to the problems that motivate this study, the morphologic dating of late Pleistocene and younger fault scarps.

Model Representation of Scarp Evolution

Homogeneous Diffusion Equation

The basic assumption underlying this study is that mass transport due to erosional processes proceeds in the downhill direction at a rate proportional to the local topographic gradient; specifically, in one spatial dimension x,

$$\dot{M} = -K\frac{\partial u}{\partial x} \tag{1}$$

where $\dot{M}$ is the rate at which mass moves downhill, $\partial u/\partial x$ is the topographic gradient normal to elevation contour, and K is the constant of proportionality. Equation (1) accounts, correctly or incorrectly, for all the physical processes that con-

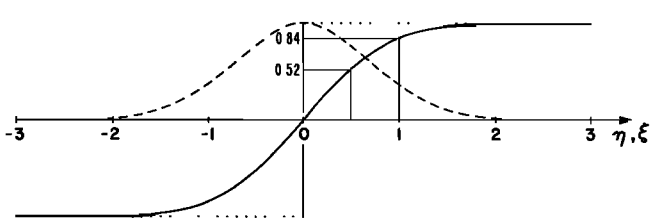

Fig. 2. The functions $e^{-\eta^2}$ (dashed) and erf (ξ) (solid), η and ξ forming the abscissa. For $\xi = x/2(\kappa t)^{1/2}$ and $t \to 0$, $\xi \to \pm\infty$ everywhere on the abscissa, driving erf (ξ) to a step-function-like "initial" condition, the dotted lines. Two numerical evaluations of erf (ξ) are given on the ordinate, erf $(\frac{1}{2}) = 0.52$ and erf $(1) = 0.84$.

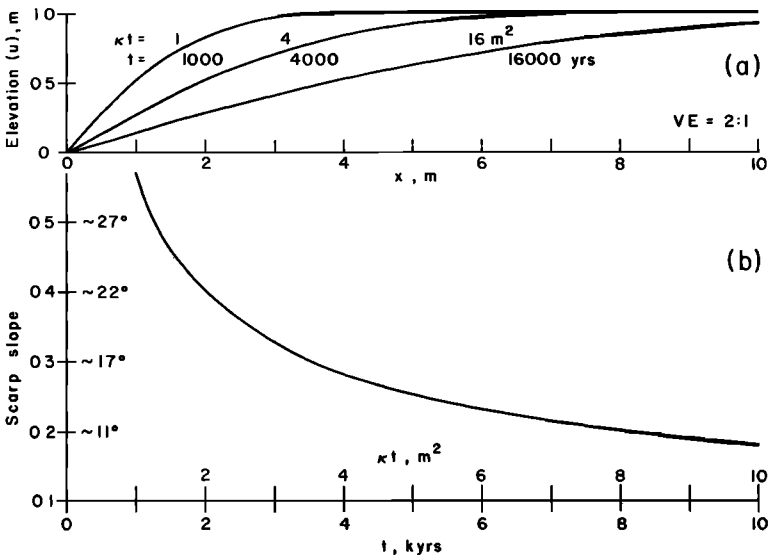

Fig. 3.(*a*) The evolution of a 2-m-high scarp ($a = 1$ m), according to (6) with $b = 0$, as a function of $x > 0$ and increasing κt. Absolute ages are determined by taking $\kappa = 1$ GKG, a value found later for the Lake Bonnville shoreline scarps. (*b*) Decay of the scarp slope, as a function of κt and t, t being determined as in Figure 3*a*. For this scarp ($2a = 2$ m) and this κ (1 GKG), degradation to the angle of repose occurs very rapidly, approximately 1000 years. A scarp twice as large has slopes twice as steep at any fixed value of κt.

tribute to erosional mass transport on the slopes of interest in this study. It is not our intention here to try to establish the validity of (1) or even to try to rationalize it in a systematic way, other than to note that gravitationally induced erosional processes on slopes should be proportional to topographic gradient for small enough slopes. *Schumm* [1967] has verified this proposition for the case of rock fragments moving downhill on exposed shale slopes in western Colorado.

The second assumption necessary for the model development is that conservation of mass holds on a local scale. This assumption is more readily justifiable than that for (1), but it does preclude dissecting erosional processes and environments. Local conservation of mass cannot be invoked for entrenched stream channels, for example; the entrenchment itself attests to mass that is now far removed from the present channel. Now, if more mass per unit time flows (in the negative x direction) across an arc element at $x + dx$ than across an arc element at x, elevation u between x and $x + dx$ will increase with time; conversely, elevation will degrade. This condition is expressed by

$$\rho \frac{\partial u}{\partial t} dx = -\frac{\partial \dot{M}}{\partial x} dx \tag{2}$$

where ρ is mass density in units of grams per square centimeter per centimeter along strike. Eliminating $\dot{M}$ from (1) and (2) yields

$$\frac{\partial u}{\partial t} - \frac{1}{\rho} \frac{\partial}{\partial x}\left(K \frac{\partial u}{\partial x}\right) = 0 \tag{3}$$

Taking K to be a material property, independent of x, t, u, or $\partial u/\partial x$, yields the homogeneous diffusion equation with constant coefficients, equation (5) below. In fact, there is little justification for taking $K = \text{const}$. It is easy to imagine K being a function of position if a scarp separates different geologic materials or a function of time if the structure in its lifetime spans significant climatic variations. Even worse, say in the evolution of a scarp in alluvial terranes, any preferential stripping of fines from the upper block (and their deposition on the lower block) will lead to time-dependent, spatial variations in K. Finally, if K depends on u or $\partial u/\partial x$, (3) becomes nonlinear, and solutions to it may not even exist.

With no a priori information about what the functional form of $K = K(x, t, u, \partial u/\partial x)$ might be, however, we have little choice but to proceed on the basis $K = \text{const}$. Setting

$$\kappa \equiv K/\rho \tag{4}$$

we then have

$$\frac{\partial u}{\partial t} - \kappa \frac{\partial^2 u}{\partial x^2} = 0 \tag{5}$$

where κ has the usual units of diffusivity. Given that it is convenient to express age of the structures of interest here in units of kiloanni (1000 years), it is convenient to express κ in units of square meters per kiloannum, a unit we denote as a GKG in recognition of the remarkable contributions of G. K. Gilbert to the matters that form the subject of this study.

In words, (5) says that when topography is convex upward, it erodes; when topography is concave upward, it forms a depositional basin for material incoming from higher elevation. Equation (5) moreover says that the rate of change of topography depends on its curvature; for the same κ, sharp features degrade faster than smooth features. All of this seems physically reasonable and, at least qualitatively, is consonant with any number of observations. The value of κ, of course, will vary according to geologic material and climatic conditions; moreover κ, at best, will be determined as an average over whatever climatic conditions are appropriate to the site of interest. Finally, we must be alert to variations of κ that may depend on either slope or differential elevation, as the latter may change along strike of the particular structure of interest.

The solution to (5) for a step of topography $2a$ imposed at $x = 0$ and $t = 0$ upon a preexisting surface of slope b (for

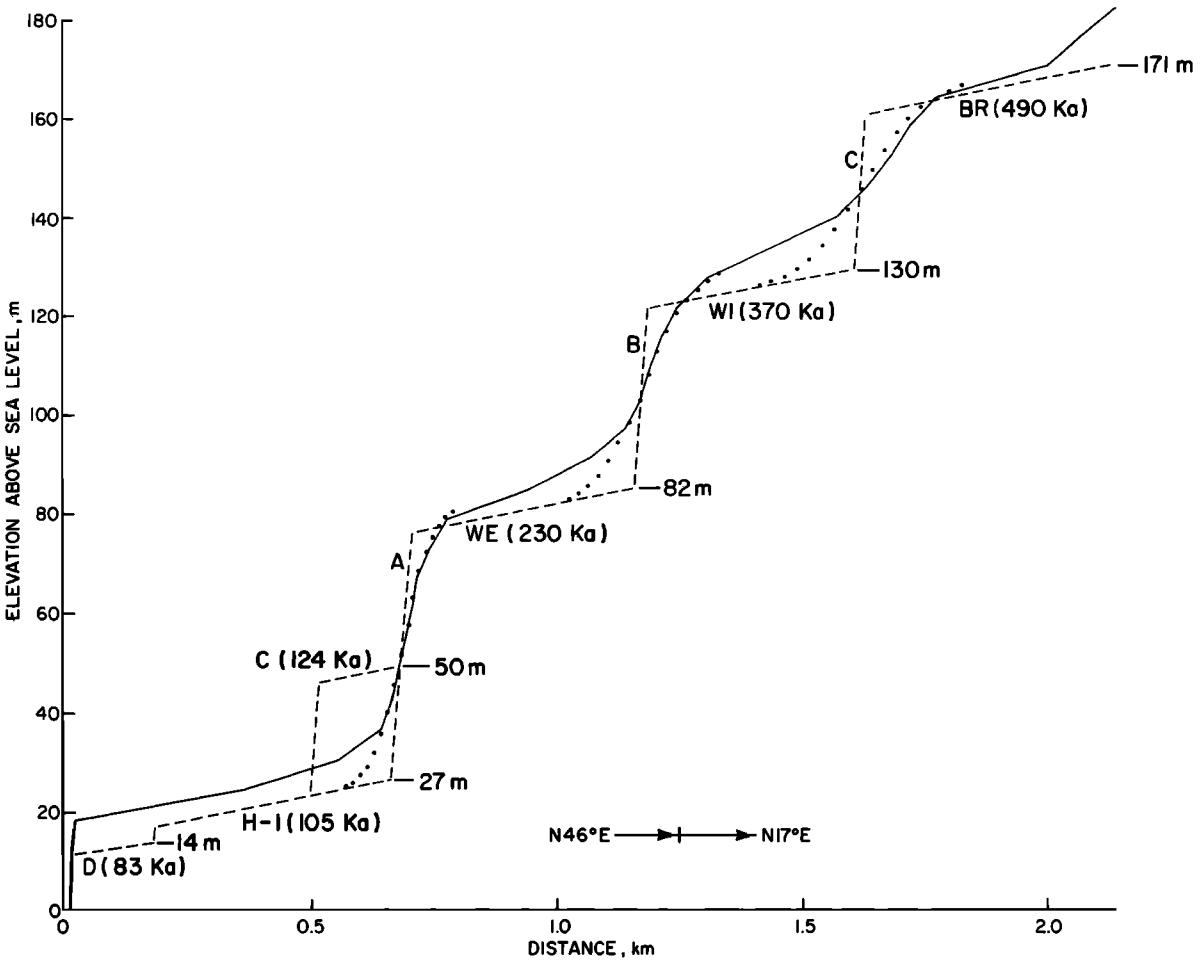

Fig. 4a. Elevation profile of the Santa Cruz sea cliffs, just east of Majors Creek. Elevation data are from the Santa Cruz 7½-min topographic sheet and are presented here at 10:1 vertical exaggeration. The azimuths and segmentation point of two straight-line profiles are shown at the bottom of the figure. The actual topography is shown as connected straight-line segments; original positions of platforms and sea cliffs (mostly from *Bradley and Griggs* [1976]) are shown as dashed lines. From lowest and youngest to highest and oldest, these platforms are (with ages in parentheses): D, Davenport; H-1, Highway 1; C, Cement; WE, Western, WI, Wilder; and BR, Blackrock. Sea cliff A, standing above the Highway 1 platform, has been assumed to have been refreshened at the time of that transgression. Sea cliffs B and C have been assigned the ages of Western and Wilder platforms, as estimated from the uplift rate of 0.35 m/ka (see text). The three sets of solid dots are model calculations for the evolution of sea cliffs A, B, and C, as discussed in the text and parameterized in Table 1.

example, a single episode of vertical, dip-slip, block faulting of a fan surface of slope b) is [e.g., *Carslaw and Jaeger*, 1959]

$$u(x, t) = a \operatorname{erf} [x/2 (\kappa t)^{1/2}] + bx \tag{6}$$

In (6), erf $[x/2(\kappa t)^{1/2}]$ is the error function of argument $x/2(\kappa t)^{1/2}$

$$\operatorname{erf}\left[\frac{x}{2(\kappa t)^{1/2}}\right] = \frac{2}{\pi^{1/2}} \int_0^{x/2(\kappa t)^{1/2}} e^{-\eta^2}\, d\eta \tag{7}$$

The maximum scarp slope angle θ_s is of much interest in detailed studies of fault scarp morphology [e.g., *Bucknam and Anderson*, 1979]. The maximum slope in this problem occurs at $x = 0$, and it is

$$\left.\frac{\partial u}{\partial x}\right|_{x=0} = \frac{a}{(\pi\kappa t)^{1/2}} + b \tag{8}$$

where we refer to $\partial u/\partial x|_{x=0}$ as the scarp slope and

$$\theta_s = \tan^{-1}\left(\left.\frac{\partial u}{\partial x}\right|_{x=0}\right) \tag{9}$$

The far-field or fan slope angle θ_f is

$$\theta_f = \tan^{-1} b \tag{10}$$

Figure 1 illustrates the geometry of the scarp slope angle θ_s, far-field slope angle θ_f, surface offset $2a$, and scarp height $2H$ (the amplitude measure used by *Bucknam and Anderson* [1979]) for a scarp perfectly antisymmetric about the origin. The scarp topography is shown here as connected straight-line segments, that is, according to the observational procedure of *Bucknam and Anderson* [1979]. While we should not expect real scarps to conform to the perfect antisymmetry of Figure 1, in fact they are often arbitrarily close to it, provided the upper slope θ_f and lower slope θ_f are well matched; mismatched upper and lower θ_f are the most frequent breakdown of antisymmetry.

An important feature of the geometry of Figure 1 is that in the presence of a nonzero far-field slope, the scarp offset $2a$ and the scarp height $2H$ are not the same (except at $t = 0$).

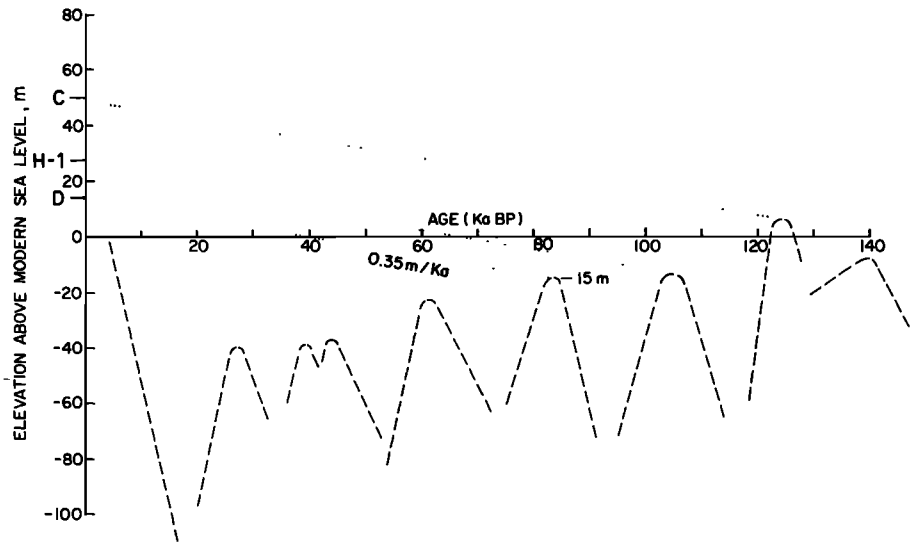

Fig. 4*b*. A space-time plot, correlating high stands of sea level existing at some time [*Bloom et al.*, 1974] with platform back edges existing at some elevation. The present elevations of the back edges of the Davenport, Highway 1, and Cement platforms are shown in Figure 4*a*. They were not cut at the same original datum, however. The correlations indicated by the dotted lines are for the same uplift rate 0.35 m/ka (slopes of the dotted lines) for all three terraces. On this basis, the ages of the Davenport, Highway 1, and Cement platforms are estimated to be 83, 105, and 124 ka, respectively.

The relation between the two is, according to the geometry of Figure 1,

$$H = a \Big/ \left[1 - \frac{\tan \theta_f}{\tan \theta_s}\right] \tag{11}$$

indicating a significant nonlinear relation between $2H$ and $2a$ whenever $\tan \theta_s$ is comparable to (it is always larger than) $\tan \theta_f$. Within the diffusion equation framework, however, it is the offset $2a$ that drives scarp modification, not $2H$.

The Source Term: Repeated Faulting

It is common to parameterize those faults that have experienced many episodes of faulting in terms of a slip rate $2A$. For uplift (and downdrop) of $U = +$ (and $-$) At, A, the rate of uplift (downdrop), becomes a pure source term for (5):

$$\frac{\partial u}{\partial t} - \kappa \frac{\partial^2 u}{\partial x^2} = A \tag{12}$$

Solutions to (12) exist for a variety of initial conditions. The one below [*Carslaw and Jaeger*, 1959, p. 79] is for an initial scarp of offset $\pm a$ at $x \gtrless 0$ cut on a preexisting surface of slope b. For $x > 0$, A corresponds to uplift, and for $x < 0$, A leads to downdrop so that $u = 0$ at $x = 0$ for all t:

$$u(x, t) = (a + At)\,\mathrm{erf}\left[\frac{x}{2(\kappa t)^{1/2}}\right] + \frac{Ax^2}{2\kappa}\left\{\mathrm{erf}\left[\frac{x}{2(\kappa t)^{1/2}}\right] - \mathrm{sgn}\,(x)\right\} + \frac{Ax}{\kappa}\left(\frac{\kappa t}{\pi}\right)^{1/2} e^{-x^2/4\kappa t} + bx \tag{13}$$

where

$$\mathrm{sgn}\,(x) = +1 \qquad x > 0$$

$$\mathrm{sgn}\,(x) = -1 \qquad x < 0$$

and a and A are now positive for all x. For this topographic function the scarp slope is

$$\left.\frac{\partial u}{\partial u}\right|_{x=0} = \frac{at^{-1/2}}{(\pi\kappa)^{1/2}} + \frac{2At^{1/2}}{(\pi\kappa)^{1/2}} + b \tag{14}$$

The second term in (14) leads to scarp slope steepening, the result of the scarp offset increasing at the rate $2A$.

Error Functions and Model Solutions

The properties of error functions are well known [e.g., *Carslaw and Jaegar*, 1959]; several are worth recounting here in the context of actually fitting topographic profiles. The error function is closely allied with the cumulative probability of a Gaussian probability distribution, although the error function is arranged to be antisymmetric about the origin with asymptotes of ± 1 as $\xi \to \pm\infty$, whereas the cumulative probability function of a Gaussian distribution is antisymmetric about the point (0, 0.5) with asymptotes 0 ($\xi \to -\infty$) and 1 ($\xi \to +\infty$). Specifically, this arrangement is

$$\mathrm{erf}\,(\xi) \equiv \frac{2}{\pi^{1/2}} \int_0^{\xi} e^{-\eta^2}\, d\eta = \frac{2}{\pi^{1/2}} \int_{-\infty}^{\xi} e^{-\eta^2}\, dn - \frac{2}{\pi^{1/2}} \int_{-\infty}^{0} e^{-\eta^2}\, dn \tag{15}$$

The first integral on the right-hand side of (15) is just twice the cumulative probability of the distribution function $e^{-\eta^2}$, and the second (negative) integral reckons to -1. Figure 2 shows the functions $e^{-\eta^2}$ (dashed) and erf (ξ) (solid).

The idea is that the solid curve in Figure 2 resembles a fault scarp profile degraded, after some elapsed time, from an initial steplike configuration given by $u = \pm 1$ for $\xi \gtrless 0$ (dots). This element of time enters our calculations through an argument of the error function representation formed of two variables, distance x away from the scarp and time t after its formation (e.g., equations (6) and (13)); that is, $\xi = x/2(\kappa t)^{1/2}$. The numerical evaluations of erf (ξ) given in Figure 2 show how the product κt can be easily estimated from actual observations. For example, say 84% of the half-scarp offset a is obtained at some measured distance X_{84}; since the 84% amplitude point

TABLE 1. Model Parameters for the Santa Cruz Sea Cliffs

Sea Cliff	$2a$, m	Age, ka	b (Upper)	b (Lower)	κt, m^2
A	50	105	0.04	0.02	1200
B	30	230	0.05	0.02	2500
C	31	370	0.03	0.02	4100

is attained when the argument of the error function is equal to 1,

$$\frac{X_{84}}{2(\kappa t)^{1/2}} = 1 \tag{16}$$

thus determining κt. If κ is known for whatever (but separate) reasons, we can date the scarp; conversely, if the age of the scarp is known, we can determine κ.

Figure 3*a* shows how a 2-m scarp ($a = 1$ m) evolves according to (6) (with $b = 0$), as a function of $x \geq 0$, κt, and t (using a value of $\kappa = 1$ GKG, a value close to what we find later for the Lake Bonneville shoreline scarps). Figure 3*a*, then, shows only the degrading part of the scarp, that with convex curvature; the aggrading portion occupying $x < 0$ is its antisymmetric equivalent (Figure 2). To illustrate the calculation at the bottom of the last paragraph, let us say that some actual scarp profile for $x > 0$ looks like the middle curve in Figure 3*a*, with an estimate of $x = 0$ fixed by the full-scarp midheight or perhaps by the point of maximum slope. The 84% amplitude is attained at 4 m, that is, $X_{84} = 4$ m; according to (16), then, $\kappa t = 4$ m^2, which, of course, is exactly the right answer in this synthetic case.

Figure 3*b* shows how the scarp slope evolves as a function of κt and t (again for $\kappa = 1$ GKG), according to (8), with $b = 0$. Irrespective of the basic validity of (1) and (2) at $\theta_s \geq \theta_r$, the angle of repose $\simeq 35°$, Figure 3*b* says that any $2a = 2$ m scarp with $\theta_s \simeq \theta_r$ in weakly consolidated alluvium must be very young indeed (less than 1 ka B.P.), if our "typical" value of $K = 1$ GKG is anywhere near correct. On the other hand, (8) implies that a scarp 5 times larger ($2a = 10$ m) will have $\theta_s \geq \theta_r$ 25 times as long, that is for some 25 ka. This makes no sense, and the problem is that fault scarps in alluvial material can be expected to degrade rapidly to θ_r irrespective of $2a$, a phenomenon not incorporated in (8). We can circumvent this problem directly by proceeding to the mathematics of finite slope, initial value scarps, as we do in our analysis of the Lake Bonneville shoreline scarps. If, however, the time for which the scarp "should" be with $\theta_s \geq \theta_r$, according to (8), is significantly less than the age of the structure, we can safely ignore this problem, and we avail ourselves frequently of this expedient.

The Data and the Models

The geomorphologic data considered in this study come in two basic forms. The first is simply elevation profiles taken normal to strike of the scarp of interest. Observations of this sort allow for a detailed assessment of the fit of model to data, at the price of some uncertainty as to how representative the particular profile is of the entire structure(s) along strike. One cannot blindly average a large suite of such profiles to obtain the "representative" profile. In the first place, all profiles must be normalized according to (6) for whatever differences in scarp offsets and/or far-field fan or terrace slopes may exist. Second, care must be taken in selecting profiles to avoid local drainage patterns, both the upslope channels and their downslope fans; mass transport of this type has been explicitly excluded by (2).

Large numbers of profiles, however, may be parameterized efficiently by point plots of the scarp slope ($\tan \theta_s$) versus the scarp offset ($2a$). These "slope-offset plots" are variations of the scarp slope angle/scarp height plots first described by *Bucknam and Anderson* [1979]. The slope-offset plots used here are restructured from the *Bucknam and Anderson* [1979] representations, so to fit explicitly within the diffusion equation analysis with which we shall interpret them. In either form, however, plots of this sort are far more representative of the structure as it may vary along strike at the expense of losing information contained in profiles away from the immediate vicinity of the scarp. This loss of information can be important, especially in the presence of nonzero and variable far-field slope b.

In this investigation we make use of both data representations, and in two cases, the Lake Bonneville shoreline scarps and the Drum Mountains fault scarps, we perform analyses in both data spaces. We begin with profile modeling, in the next section, of the Santa Cruz sea cliffs, the Raymond fault, the Lake Bonneville shoreline scarps, and the Drum Mountains fault scarps; then we turn to the slope-offset analysis of the Lake Bonneville shoreline scarps and four sets of fault scarps in west-central Utah, those at the Drum Mountains, Fish Springs Range, Oquirrh Mountains, and Sheeprock Mountains. In the discussion section, we bring these results together, emphasizing the advantages and disadvantages of the slope-offset plots.

Profile Modeling

The Santa Cruz sea cliffs. South and west of Santa Cruz, California, a series of marine terraces ascends the south facing slope of Ben Lomond Mountain adjacent to the Pacific Ocean. These terraces were cut by wave action during intermittent glacioeustatic high stands of sea level, as the coastline was tectonically uplifted during Quaternary time. The original configuration of each terrace was presumably similar to that of the terrace being cut today at the modern sea level, a nearly horizontal wave-cut platform backed by a nearly vertical, seaward facing sea cliff. The emergent sea cliffs have degraded with time, and the resultant erosional debris has covered the platforms below them with thin aprons of alluvium and colluvium. *Bradley and Griggs* [1976] discuss these emergent platforms in some detail, and their results figure prominently in our age determinations and initial condition assignments for the numerical modeling below.

From highest (oldest) to lowest (youngest), these terraces are, as named by *Bradley and Griggs* [1976], Quarry, Blackrock, Wilder, Western, Cement, and Santa Cruz. The Santa Cruz terrace consists of two wave-cut platforms, the Highway 1 platform (higher and older) and the Davenport platform (lower and younger), both presently covered (Figure 4*a*). At no place does a topographic profile perpendicular to the coast intersect all six terraces in the sequence. For this study we use a topographic profile just southeast of Majors Creek where the Blackrock, Wilder Western, and Santa Cruz terraces are well preserved (Figure 4*a*). For dating purposes we project the Cement platform/cliff pair onto this profile, using the relative elevations of the terraces 9 km to the northwest.

Bradley and Addicott [1968] have reported U series ages of 76,000 ± 800 and 95,500 ± 700 years for the two fossil mollusk localities on the Davenport platform. *Kennedy et al.*

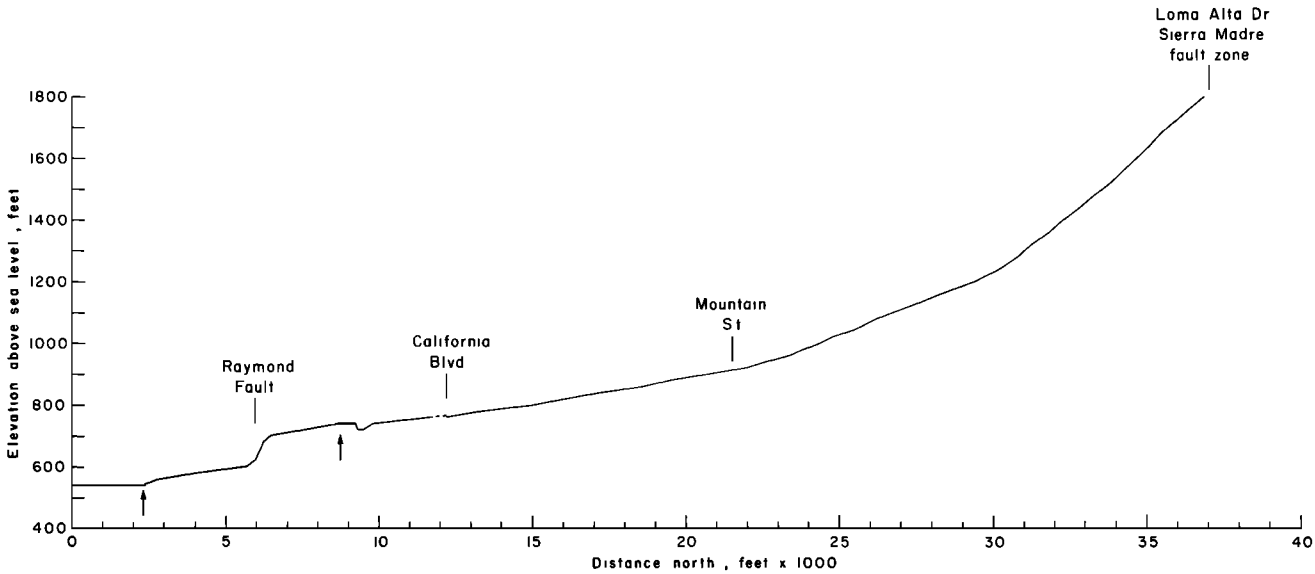

Fig. 5. North (right)/south (left) elevation profile across the northern San Gabriel Valley. From south to north the profile traverses the Raymond Basin south of the Raymond fault and the Altadena alluvial slope north of it. To the north the profile is truncated at the Sierra Madre fault zone beyond which lie the San Gabriel Mountains. Elevations are taken from the 7½-min topographic sheets for Pasadena and Los Angeles and are presented here at a 10 :1 vertical exaggeration. North of California Boulevard, the elevation is along Lake Avenue, a nearly north-south line. South of California Boulevard, the elevation is along a north-south line intersecting California one block west of Lake, to minimize the affect of a local drainage due south of the intersection of Lake and California. The vertical arrows north and south of the Raymond fault indicate breaks in the far-field slopes of possible significance with respect to ancient offsets across the Raymond fault (see text). The topography adjacent to the Raymond fault between the 560 and 740 ft elevation contours is enlarged in Figure 6.

[1982] assign an age of 83 or 105 ka to the Davenport platform, using amino acid racemization data for the fossil mollusks and their cool water faunal aspect. Assuming that the Davenport platform was cut during the relative high stand of sea level 83 ka B.P. (Figure 4*b*) and also that the sea level curve of *Bloom et al.* [1974] is appropriate, we conclude that the Davenport platform was cut 15 m below modern sea level. At Majors Creek the Davenport platform is presently 14 m above modern sea level; it has thus been uplifted 29 m in the past 83 ka, at an average uplift rate of 0.35 m/ka. If this uplift rate is valid for the past 124 ka, the Highway 1 platform and the Cement platform correlate well with the 105 and 124 ka sea level high stands, respectively (Figure 4*b*).

The close agreement between the relative elevations of the three lowest platforms and those of the three prominent peaks on the sea level curve suggests that the assumption of constant uplift is valid over the last 124 ka. If we project the uplift rate of 0.35 m/ka beyond 124 ka B.P., we obtain tentative ages of 230 and 370 ka for the Western (82 m) and Wilder (129 m) platforms, respectively.

The subsurface geometry of the buried wave-cut platforms are known in some detail [*Bradley and Griggs* 1976], both from detailed mapping of platform exposures and from shallow seismic refraction studies. The positions of their associated sea cliffs are known less certainly except where they are exposed in section by major drainages. In such exposures the original sea cliffs are closely aligned with the scarp midheight; we have placed them there with attitudes the same as the modern sea cliff. Finally, in drawing the platforms we have ignored the slight difference in slope between the inshore and offshore segments [*Bradley and Griggs*, 1976]. These platform/cliff positions are shown as dashed lines in Figure 4*a*. All of them are cut into the Pliocene Santa Cruz Mudstone, which, according to *Bradley and Griggs* [1976] "is thinly bedded and highly jointed, which expedites wave erosion and stream incision, but its siliceous nature retards decomposition once platforms are stranded on the interfluves."

Inspection of Figure 4*a* indicates that there is far more mass on any platform than could possibly be derived from erosion of the upper half of its facing sea cliff. This "excess mass" could be the result of windblown sand accumulating on the lower platform or debris deposited as interlacing fans as a result of streams incised into higher standing sea cliffs; it is unlikely to be due to parallel retreat, unless the sea cliffs along this profile have retreated 50 m or more from their original stands (which is not suggested by the stream exposures). In any event, this "mass excess" is not accounted for in our model calculations.

What confuses matters is that this "excess mass" imparts far-field slopes to the Western and Wilder terraces significantly greater than those of their underlying platforms. To reckon with this difficulty, we simply choose different upper and lower far-field slopes, that of the lower platform for the lower slope and that of the modern topography for the upper slope. This expedient makes our model calculations in the far field look nicer than they would have been had we chosen a single b for both upper and lower slopes (e.g., Figure 6), but otherwise it is of not much consequence; what matters is where the topography has curvature, not where it has more or less constant slope.

The parameters for the model calculations (equation (6)) are given in Table 1. Cliff ages are taken to be the age of the platform beneath, and we have assumed that sea cliff A was refreshened at the time of the Highway 1 transgression. The estimates for 2*a* are scaled directly from the appropriate cliff/platform geometry, and the upper and lower far-field slopes

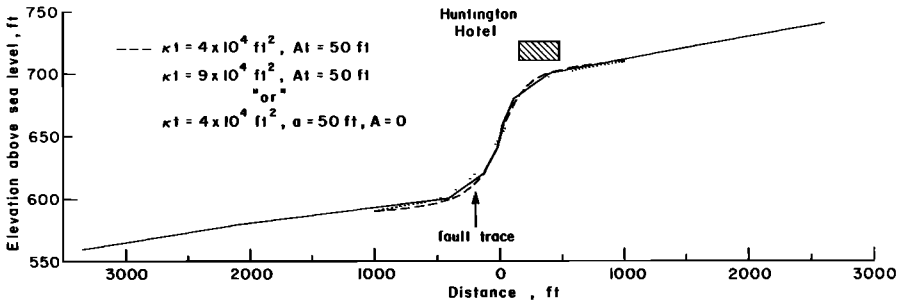

Fig. 6. An enlarged view of the topography local to the Raymond fault, along the same profile as in Figure 5; vertical exaggeration is again 10:1. This line passes through the Huntington Hotel, the lateral position of which is correct; it is removed vertically from the topography for clarity and is not drawn to correct vertical scale. The model calculations described in the text are parameterized in the figure as indicated.

are measured as described in the preceding paragraph. The value $\kappa t = 2500$ m^2 was estimated for the degrading portion of sea cliff B with (16). For $t = 230$ ka, this yields $\kappa = 11$ GKG, and we have used this value for each of the three model calculations (solid dots) in Figure 4*a*. The origin of coordinates for each model calculation has been placed at the sea cliff midheight.

The model calculations are in close agreement with the actual elevation profiles across the degrading portions of sea cliffs A and B; in the case of sea cliff C the model fit for the upper slope would be improved with a slightly larger κ ($\sim$40% larger). On all three of the lower platforms, however, a mass excess exists, a problem we knew of in the absence of model calculations. The noteworthy aspect of the model calculations is that reasonble agreement between the actual and model elevation profiles for all three sea cliffs has been obtained with the same κ. Barring some untoward coincidence of offsetting variations in κ and the age estimates, we may conclude that the relative ages between cliffs A, B, and C are fairly well determined, to the extent they may be estimated from model fits to the degrading section alone. So, too, are their absolute ages, if we may regard the age of cliff A as being safely bounded by the 83 and 124 ka transgressions. Thus, for example, while our model calculations are not sensitive enough to determine whether cliff B is really 200 or 300 ka (as opposed to the estimated age of 230 ka), we feel confident that it is not 400 ka. In this case, cliff B would have an elevation profile quite similar to cliff C. Similarly, it seems likely that cliff B must be 2–3 times the age of cliff A, neither much older or much younger.

To assess the validity of the vertical initial value scarp model, we estimate the time for which sea cliffs A, B, and C "should" have had $\theta_s \geq \theta_r \simeq 35°$ to be 42, 15, and 15 ka, respectively, using (8), the parameters of Table 1, the upper slope b values, and $K = 11$ GKG. In the case of sea cliffs B and C these times are indeed small compared to the total age of the structures. In the case of sea cliff A this time is about 40% of the inferred (refreshened) age of sea cliff A. This leads to some bias in the true κt for sea cliff A with respect to our estimate in Table 1 based on (6), but one that is less than a factor of 50%, as we shall see when we deal with the Lake Bonneville shoreline scarps in terms of the finite slope, initial value problem.

The Raymond fault. Since middle Pleistocene time, the northern San Gabriel Valley has accumulated hundreds of meters of coarsely sorted alluvium, the erosional debris from the San Gabriel Mountains standing just to the north across the Sierra Madre fault. Most of this material has been emplaced in the form of large, often interlacing, effluent fans, the older ones left-laterally offset from their parent streams by the Sierra Madre fault, across which significant uplift has occurred as well. Figure 5 shows the north-south elevation profile of the Altadena alluvial slope, which is bounded on the north by the Sierra Madre fault and on the south by the Raymond fault.

Structurally, this surface is old, perhaps a million years or more. It is built from the alluvial units 4 and 3 described by *Crook et al.* [1983], the former thought to have accumulated from the middle Pleistocene to about 2×10^5 years ago, while the overlying unit 3 accumulated between $\sim 2 \times 10^5$ and $\sim$ 11,000 years ago. An uncomformity separates the two units, expressed in the ancient soils developed on unit 4. Locally, the Altadena alluvial slope is covered by even younger deposits.

The topography local to the Raymond fault is plainly much younger, and it is this youthful feature we analyze below. *Crook et al.* [1983] present detailed geologic information on the history of the Raymond fault, as part of a larger study to assess the recency and rate of fault activity in this region. Notably, the present-day topographic relief ($\sim$30 m) of the Raymond fault is only a fraction of the total vertical offset across it, variously estimated to be 135 m to as much as 775 m, estimates recounted by *Crook et al.* [1983]. Figure 6 presents a view enlarged from Figure 5 of the topography local to the Raymond fault.

The three model calculations in Figure 6 are all derived from the solution to the repeated faulting problem (13). This solution is specified by the parameters a, b, κt, and At, A/κ then being determined; $b = 0.01$ is a close approximation to the lower far-field slope, but the upper far-field slope is almost twice this much. Here we use $b = 0.01$ for both the upper and lower far-field slopes to illustrate the effect this parameter has, should one estimate it incorrectly by a factor of 2. The first model (dashed line) is the preferred fit; for it, $a = 0$, $\kappa t = 4 \times 10^4$ ft^2 (3.7×10^3 m^2), and $At = 50$ ft (15.2 m). That is, we have assumed that there was no initial scarp and that the total offset $2At = 100$ ft (30.5 m) has accumulated at rate $2A$ since the time ($t = 4 \times 10^4$ ft$^2/\kappa$ (3.7×10^3 m$^2/\kappa$)) the present topography began to form. This model closely fits the observed topography within 1000 ft (305 m) of the origin, taken (as always) at the scarp midheight. For $|x| < 1000$ ft (305 m), the misfit is never greater than 5 ft (1.5 m) and generally is considerably less than that; indeed, most of it may be due solely to the connected straight-line representation of the actual elevation. At greater distances, the misfit is greater, entirely the

Fig. 7. Shoreline scarp of glacial Lake Bonneville, cut by wave action some 14,500 years ago into an alluvial fan at the mouth of Long Canyon, west flank of the Gilson Mountains, Juab County, Utah. The scarp here is about 15 m high.

effect of mismatched far-field slopes with respect to the choice of $b = 0.01$.

The other two models simply illustrate what can be resolved in calculations such as these. The second model (dotted line) is the same as the first except that κt has been increased by a factor of 2.25, to 9×10^4 ft^2 (8.4×10^3 m^2). This is plainly a poorer fit to the Raymond fault topography, and we conclude that κt can be readily determined with less uncertainty. As we shall see in the two following sections, κt is resolvable at the 50% level of uncertainty when detailed topographic observations are available. The third model calculation, which is indistinguishable from the second at the scale of the dot size of Figure 6, is preposterous geologically but is of interest with respect to the effect that repeated faulting has on the scarp slope. In this model, $\kappa t = 4 \times 10^4$ ft^2 (3.7×10^3 m^2) as in the first model, but $A = 0$ and $2a = 100$ ft (30.5 m), that is, this model treats the Raymond fault as an initial value problem, with all 100 ft (30.5 m) of offset occurring at the remote time $t = 4 \times 10^4$ ft$^2/\kappa$ (3.7×10^3 m$^2/\kappa$). This model illustrates how repeated faulting has a significant effect in steepening the scarp slope, more precisely, in keeping it steep.

Crook et al. [1983] have identified and dated five major seismic events on the Raymond fault since 36 ka B.P. from exposures in three trenches, two of them at Lacy Park within 0.5 km of the intersection of the elevation profile with the Raymond fault. With some allowance for evidence of three additional but undated events and undetected events in the same interval, they have inferred an average recurrence interval of about 3000 years for events with an average vertical displacement of 0.4 m, which yields $2A = 0.13$ m/ka. For the preferred model with $At = 50$ ft (15.2 m) and $\kappa t = 4 \times 10^4$ ft^2 (3.7×10^3 m^2), $\kappa/A = 0.8 \times 10^3$ ft = 240 m and $\kappa = 16$ GKG. Assuming that the average uplift rate since 36 ka B.P. is valid for the entire history of the modern topography which, if nothing else, is consistent with the model calculation, we estimate that the modern topography began to form about 230,000 years ago.

With $a = 0$ and values of A, κ, and b as presented above, (14) says that the Raymond fault has never been at $\theta_s \geq \theta_r$ (and will not be for another 1200 ka). A worst case analysis is that this scarp formed as a single event. For $a = 15$ m, $\kappa = 16$ GKG, $b = 0.01$, and $A = 0$, (14) (now reduced to (8)) yields 9.4 ka as the time for θ_s to degrade to θ_r, a negligible fraction of the age of the Raymond fault.

The model tells us, then, at 230 ka B.P., there should have been little if any topographic expression along the Raymond fault, and yet we can safely surmise that a hundred meters, if not hundreds of meters, of offset across the Raymond fault had already accumulated by that time. What became of the topographic expression of these more ancient faulting displacements?

In the first place, there is, just possibly, evidence for this ancient topographic expression in the breaks in slope on either side of the Raymond fault, at 2800 ft (853 m) north of the fault and at 3600 ft (1097 m) to the south (Figure 5, vertical arrows). In any event, however, this ancient relief on the Raymond fault and most if not all of its topographic expression away from the fault must have been leveled or buried near the end of unit 4 time; our model age for the modern topography is nearly coincident with the unit 4/unit 3 unconfirmity. This leveling/burial event must have been a dramatic, and very complete, event somewhere near the end of unit 4 time, such that so much fault offset has left so little expression at the present time. A fault scarp of 100 or more meters high, even if it were many hundreds of thousands of years old would, roughly speaking, appear today as a greatly exaggerated version of sea cliff C (Figure 4*a*), given the two nearly coincident values of κ.

The Lake Bonneville shoreline scarps. The precipitous lowering of ancient Lake Bonneville through Red Rock Pass 14,000 to 15,000 years ago [*Scott et al.*, 1982] stranded numerous wave-cut shoreline scarps throughout much of western Utah (Figure 7). The Lake Bonneville shoreline and associated scarps have figured prominently as absolute age, topographic,

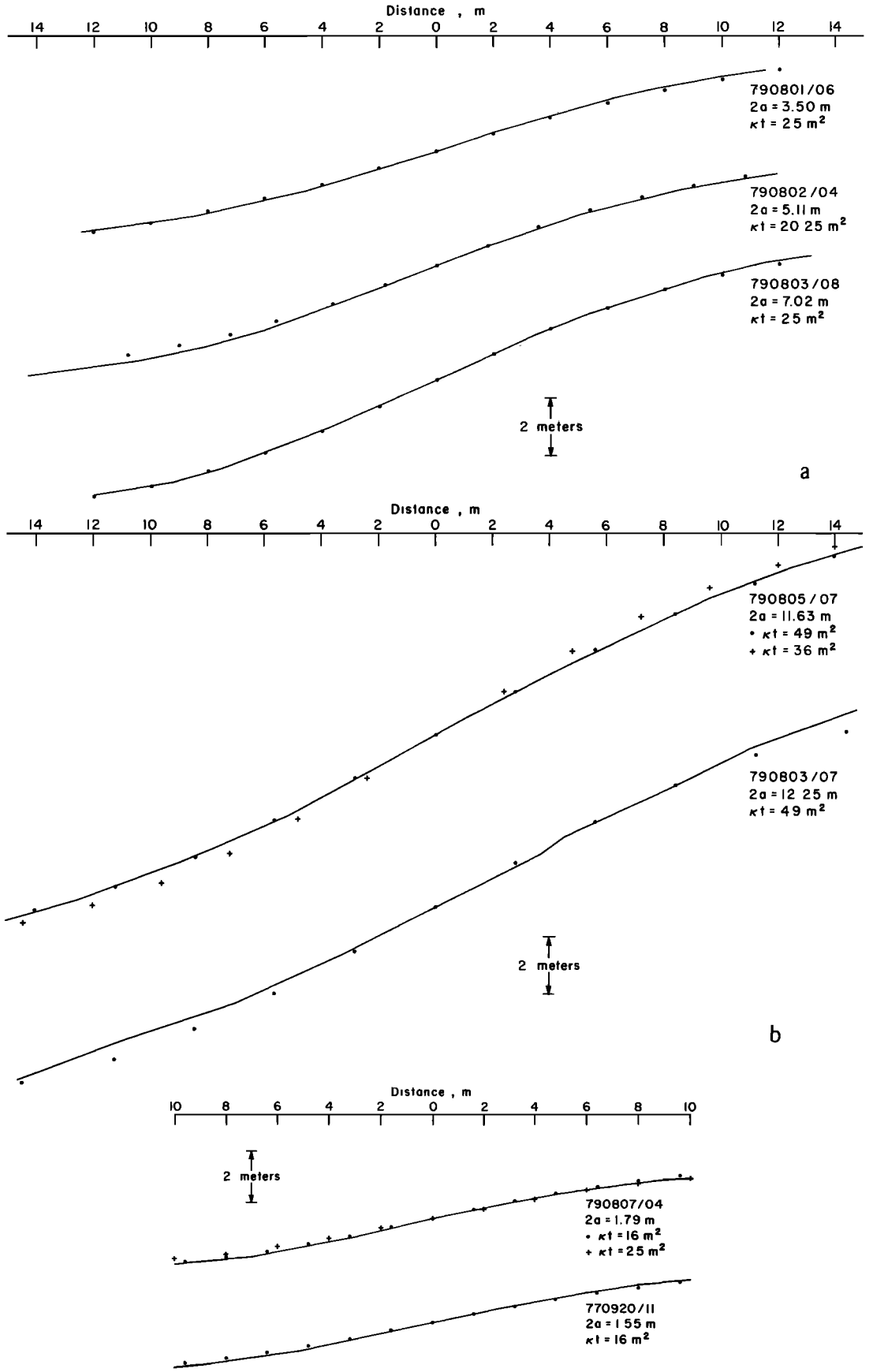

Fig. 8. Elevation profiles of Lake Bonneville shoreline scarps. The actual topography is shown as straight-line segments, the model calculations by point symbols. The profiles are identified by the year, month, and day they were taken; their offset $2a$; and model value of κt. (*a*) Intermediate-sized scarps ($2a$ = 3.50, 5.11, 7.02 m). (b) Large scarps ($2a$ = 11.63, 12.25 m). (*c*) Small scarps ($2a$ = 1.79, 1.55 m).

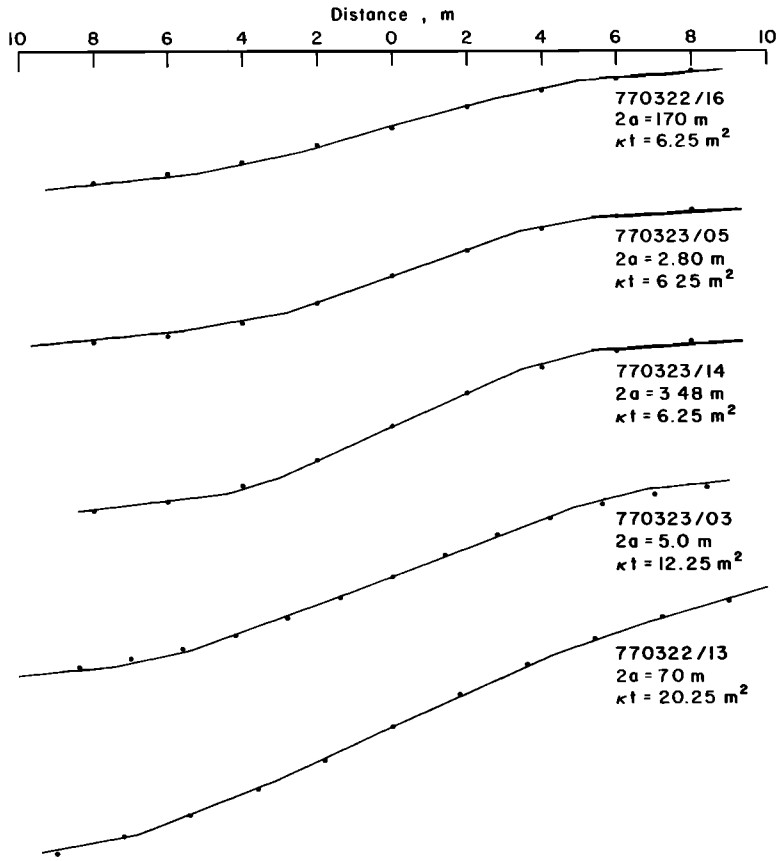

Fig. 9. Five elevation profiles of the Drum Mountains fault scarps. Topography, model calculations, profile identification, and model parameterizations are the same as in Figure 8.

and isostatic control points for geologic processes operative in the Basin and Range Province since the geologic manifestations and history of Lake Bonneville were described in the monumental work of *Gilbert* [1890].

Sixty one cross-strike topographic profiles of the Bonneville shoreline scarps are presently available; this data set spans more than an order of magnitude variation in $2a$ ($1.01 \leq 2a \leq 12.25$ m). Seven of these topographic profiles are grouped in Figure 8 according to intermediate values of $2a$ (3.50, 5.11, and 7.02 m, Figure 8*a*), large values of $2a$ (11.63 and 12.25 m, Figure 8*b*), and small values of $2a$ (1.79 and 1.55 m, Figure 8*c*). The topography, determined from detailed leveling measurements obtained in the manner of *Bucknam and Anderson* [1979], is shown as the connected, straight-line segments. The model calculations (all based on equation (6)) are shown as point symbols. The quantities a and $b = \tan^{-1}(\theta_f)$ are determined from the leveling measurements themselves in the manner of Figure 1; the origin of coordinates is fixed at the point of the offset midheight.

In general, these model fits represent a single guess at κt through (16), rounded to a convenient square number so to expedite calculations performed with a slide rule and the table of error functions from *Carslaw and Jaeger* [1959, p. 485]. Even so, it has usually been possible to reproduce the actual topography with a maximum misfit of no more than several percent of the full-scale topographic range. Moreover, the maximum misfit almost always occurs at one end of the profile or the other, almost surely the result of slightly mismatched upper and lower far-field slopes. The elevation difference, for example, between a 4° and 5° slope at 10 m distance is 17 cm, although we generally do better than this in Figure 8. In any event, the topography in Figure 8 can be very closely matched by error functions, with the possible exception of the bottom profile in Figure 8*b*.

The intermediate-sized scarps in Figure 8*a* all suggest a value of κt near 25 m^2. The upper and lower profiles are closely matched by the model calculations, as is most of the intermediate profile. The misfit along the lower one third of the middle profile is in the vicinity of 5% of the full-scale topography. The value of κt for this profile is somewhat lower as well (20.25 m^2).

The product κt is larger for the larger scarps, however (Figure 8*b*). The upper profile is closely matched by $\kappa t = 49$ m^2, everywhere at the 1% level or less. A model calculation with $\kappa t = 36$ m^2 is shown for comparison and is plainly a poor fit to the observations. The lower scarp in Figure 8*b*, and the largest in the entire data set, is harder to fit, in part because of the topographic kink 4 m to the right of midheight. A choice of $\kappa t > 49$ m^2 (the model value, Figure 8*b*) would improve the fit for the lowermost part of the scarp but would degrade the fit for the uppermost part. However poor the model fit is to the lower scarp in Figure 8*b*, however, it too suggests a $\kappa t \simeq 49$ m^2, again significantly larger than $\kappa t = 25$ m^2 obtained for the intermediate-sized scarps.

This dependence of κt on $2a$ is also apparent in the smaller scarps (Figure 8*c*). The model results for the smaller scarps imply that $\kappa t \simeq 16$ m^2, compared to $\kappa t = 25$ m^2 for the intermediate-sized scarps. For the smaller scarps, however, the matter is less well-resolved, since κt is harder to fix with certainty for the smaller scarps. The top scarp in Figure 8*c* is fit

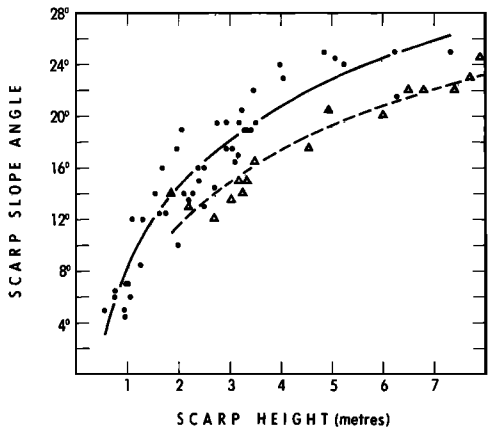

Fig. 10. Scarp slope angle/scarp height plot for Lake Bonneville shoreline scarps (open triangles) and Drum Mountains fault scarps (solid circles). Solid triangles denote overlapping shoreline and fault data. The smooth curves are of the functional form of equation (17) in the text. From *Bucknam and Anderson* [1979].

almost as well with $\kappa t = 25$ m^2 as with $\kappa t = 16$ m^2. At this level of detail, even minor uncertainties in the origin of coordinates and/or b estimates are important.

The appearance here is one of nonlinear modification processes; κ apparently depends on $2a$, since all of these scarps are of the same age. The problem, however, is the one we alluded to earlier in the discussion of Figure 3*b*. Had, for example, $\kappa t = 25$ m^2 indeed been appropriate for a 12-m-high Lake Bonneville shoreline scarp, it would yet have a slope angle beyond the angle of repose. Specifically, we estimate $\partial u/\partial x|_{x=0} = 0.77$ (that is $\theta_s = 38°$) from (8), using $a = 6$ m, $b = 0.09$ (a typical fan surface slope for the Bonneville shoreline scarps), and $\kappa t = 25$ m^2. Fourteen thousand plus years after such a scarp was formed in weakly consolidated alluvium, it hardly seems reasonable that it would stand beyond $\theta_r \simeq 35°$. We shall return to this problem in the section on the slope-offset plots, where we shall treat it in terms of the finite slope, initial value scarp, but first we conclude our profile modeling with an analysis of cross-strike elevation profiles of a set of nearby fault scarps of unknown age.

The Drum Mountains fault scarps. Some 30 km northwest of Delta, Utah, a swarm of normal fault scarps cuts a fan surface built on the east flank of the Drum Mountains. According to *Bucknam and Anderson* [1979], these scarps are less than 12,000 years old, lying as they do beneath the Provo II level of Lake Bonneville. On the basis of *Scott et al.* [1982], we take the above date to be 13.5 ka B.P. in this study. Moreover, several of the scarps cut a bar formed at the Provo II level, and these are apparently unmodified by wave action. *Bucknam and Anderson* [1979] presented 49 scarp slope angle/scarp height pairs, observations we reconsider in a slope-offset plot in a later section. These morphologic observations are also consistent with the geologic constraints that the Drum Mountains fault scarps are younger than the Lake Bonneville shoreline scarps.

An unusual feature of these fault scarps is their cross-strike spread; they form a band some 30 km long and 5 km wide, the width of this zone pointing to a complicated near-surface faulting geometry. If these faults were all formed at the same time, they moreover suggest a complicated and unusual faulting process. While these scarps need not have formed all at the same time, we do know that they are all young, less than 13.5 ka; moreover, they show no geomorphic expression of having been multiply faulted.

Figure 9 shows cross-strike elevation profiles for five of the Drum Mountains fault scarps. Scarp offsets $2a$ vary from 1.70 to 7.0 m, the largest scarp in the data set. The top three scarps ($2a = 1.70$, 2.80, and 3.48 m) are all closely fit by equation (6), and $\kappa t = 6.25$ m^2 is recovered for them all. For the same reasons as in the preceding section, κt is least well resolved for the smallest scarp, and $\kappa t = 4$ m^2 works almost as well as $\kappa t = 6.25$ m^2 for it. Recalling that $\kappa t = 16$–25 m^2 for comparably sized Lake Bonneville shoreline scarps and assuming that κ is the same for both sets of $2a < 4$ m scarps, we estimate that the smaller Drum Mountains fault scarps are 3–4 times younger than the Lake Bonneville shoreline scarps, namely, 3500–5000 years in age.

As is evident from even casual estimates of X_{84}, the two larger scarps ($2a = 5.0$ and 7.0 m) require larger values of κt, the model values being 12.25 and 20.25 m^2, respectively. For these scarps, however, there are several possible explanations. First, they may be explained by the finite slope, initial value problem, as suggested above for the Lake Bonneville shoreline scarps. Second, they may be truly older than the smaller scarps. Third, they may have been multiply faulted, the absence of evidence ordinarily accepted for multiple faulting notwithstanding. Finally, they may be subject to nonlinear modification processes leading to a larger κt, even if they were formed at the same time as the smaller Drum Mountains fault scarps. We address these possibilities when we reconsider the Drum Mountains fault scarp data in the slope-offset plot.

The Slope-Offset Plots

Bucknam and Anderson [1979] described and employed an efficient parameterization of profile data from which comparative age dating of scarps could be obtained. This is the scarp slope angle/scarp height plot, and Figure 10 reproduces the first one made, which compares such observations for the Lake Bonneville shoreline scarps and the Drum Mountains fault scarps [*Bucknam and Anderson*, 1979, Figure 4]. At any scarp height the fault scarps have greater scarp slope angles than do the shoreline scarps; the idea is that since the former are steeper, they are fresher and younger than the latter. This notion is consistent both with the geological constraints of *Bucknam and Anderson* [1979] and with the profile modeling results of the last two sections.

Bucknam and Anderson [1979] moreover inferred a logarithmic relation between scarp slope angle θ_s and scarp height $2H$ (Figure 1), and the curves in Figure 10 are regressions of θ_s on $2H$ according to the relation

$$\theta_s = C_1 + C_2 \log (2H) \tag{17}$$

where θ_s is in degrees and $2H$ is in meters. Beginning with Figure 5 of *Bucknam and Anderson* [1979], the standard representation of such data has become semilogarithmic plots of θ_s versus $2H$, so to reduce (17) to sets of staight lines, one for each set of scarps of interest [*Mayer*, 1982; *Machette*, 1982].

The principal limitation of the form (17) is that it precludes the use of the one datum that is model-independent; specifically, according to any realizable model of scarp modification whether it be (5) or anything else, we must be able to recover the far-field slope angle θ_f in the limit of vanishing scarp

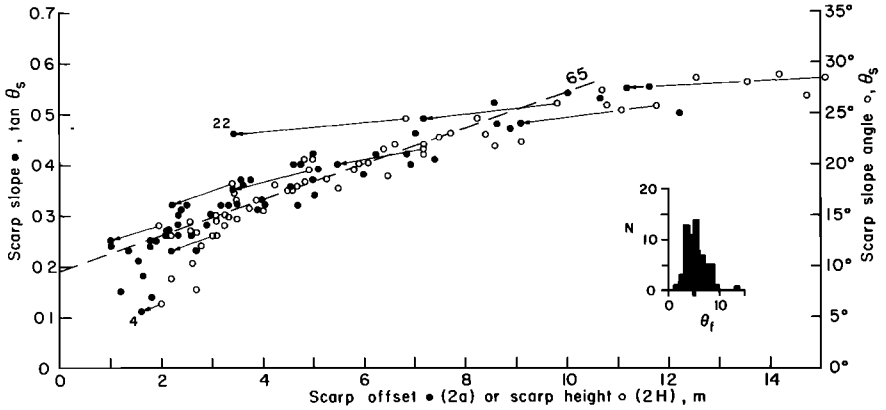

Fig. 11. The scarp slope angle/scarp height (open circles) and slope-offset (solid circles) representations of the Lake Bonneville shoreline scarps. The arrows from an open circle to a solid circle trace typical trajectories between the different representations of the same profile. These vectors arise mainly from the differences between $2a$ and $2H$ for the same scarp (Figure 1 and equation (11)), since the linear transformation $\theta_s = 55 \tan \theta_s$ is a very close approximation at these small angles ($\leq 30°$). For convenience of plotting, however, the linear transformation between the right-hand and left-hand scales is $\theta_s = 50 \tan \theta_s$. The dashed straight line yields $\kappa t = 65$ m^2 and $b = 0.19$, the inverse tangent of which is 11°. This is about twice the center of the fan slope angle distribution (inset, where N is frequency of occurrence and θ_f is in degrees).

height. Equation (17) does not allow us to recover this "intercept value," but (8) does, and we recall it here:

$$\left.\frac{\partial u}{\partial x}\right|_{x=0} \equiv \tan \theta_s = \frac{a}{(\pi\kappa t)^{1/2}} + b$$

which returns us to the restrictions of the diffusion equation representation of a single, vertical scarp-forming event at $t = 0$. The application of (8) to actual observations, however, requires a restructuring of the *Bucknam and Anderson* [1979] representation. In the first place, it is tan θ_s that is to be plotted on the ordinate, not θ_s; in the second place, it is a (or $2a$) that is to be plotted on the abscissa, not $2H$. As we emphasized earlier (equation (11) and Figure 1), these two amplitude measures are not the same in the presence of nonzero b. Finally, in the presence of variable b, it is to be recognized that even the same set of scarps of the same age is not to be represented by one line in the slope-offset plane but by a family of parallel lines, one for each significantly different b. That is, variable b introduces systematic scatter to the slope offset plot. Two structures have different ages, more precisely different products of κt, only if their respective tan $\theta_s - 2a$ lines have different slopes.

Figure 11 illustrates how the transformation from the $\theta_s - 2H$ representation (open circles) to the tan $\theta_s - 2a$ representation (solid circles) works for all 61 Lake Bonneville shoreline observations. Arrows connecting an open circle to a solid circle show how the two different point representations of the same profile differ for several different trajectories. In this linear space, the tan $\theta_s - 2a$ representation eliminates most, but not all, of the curvature in the $\theta_s - 2H$ representation. Although it is easier to illustrate the effect of variable b in other, more manageable slope-offset plots, we note here that the solid circles labeled 4 and 22 come from profiles with the smallest ($\theta_f = 1.8°$) and largest ($\theta_f = 13.0°$) fan slope angles, respectively, in the entire Lake Bonneville data set.

Consistent with (8), we offer a straight-line "fit" (dashed line) to the slope offset data (solid circles) in Figure 11. Although this is not a bad fit to the observations, especially in the range $2 \lesssim 2a \lesssim 9$ m, it is also clear that scarp slopes for both $2a < 2$ m and $2a > 9$ m fall noticeably below this straight line (suggestive of the $\kappa t - 2a$ dependences of which we spoke earlier). Another problem is that the slope of this dashed line yields $\kappa t = 65$ m^2, larger than any value obtained in the section on profile modeling ($\kappa t = 16$ to 25 m^2 for $2a < 2$m; $\kappa t = 25$ m^2 for $3.5 \leq 2a \leq 7$ m; $\kappa t \simeq 49$ m^2 for $2a \geq 10$ m). Even worse, the intercept value of this straight line is $b = 0.19$ or $\theta_f = 11°$, twice the average fan slope of 5°–6° (inset of Figure 11). What we need now to interpret the Lake Bonneville shoreline slope-offset data in particular and to work in the slope-offset plot in general is the slope-offset relation for the finite slope, initial value scarp.

A very general solution to the homogeneous diffusion equation (5) for any antisymmetric initial topography $f(x') = -f(-x')$ is

$$u(x, t) = \frac{1}{2(\pi\kappa t)^{1/2}} \int_0^\infty f(x')\{\exp[-(x - x')^2/4\kappa t] - \exp[-(x + x')^2/4\kappa t]\}\, dx' \qquad (18)$$

with $u(-x,t) = -u(x,t)$ [*Carslaw and Jaeger*, 1959, p. 59]. At any time t, the scarp slope for this topography is, differentiating (18) and setting $x = 0$,

$$\left.\frac{\partial u}{\partial x}\right|_{x=0} = \frac{1}{2(\pi)^{1/2}} \frac{1}{(\kappa t)^{3/2}} \cdot \int_0^\infty x' f(x') \exp(-x'^2/4\kappa t)\, dx' \qquad (19)$$

We suppose that the scarp forms as a ramp function with slope α for $|x'| \leq |x_1| = a/\alpha$, where a is the half-scarp offset as before and that this scarp-forming event occurs on a preexisting surface of uniform slope $\beta = b$. Then

$$f(x') = \alpha x' \qquad |x'| \leq |x_1| = a/\alpha \qquad (20a)$$

$$f(x') = \pm a + \beta x' \qquad |\pm x'| \geq |\pm x_1| = a/\alpha \qquad (20b)$$

Substituting equations (20) at $x' \geq 0$ into (19) and integrating yields

$$\left.\frac{\partial u}{\partial x}\right|_{x=0} = (\alpha - \beta)\, \mathrm{erf}\left[\frac{a/\alpha}{2(\kappa t)^{1/2}}\right] + \beta \qquad (21)$$

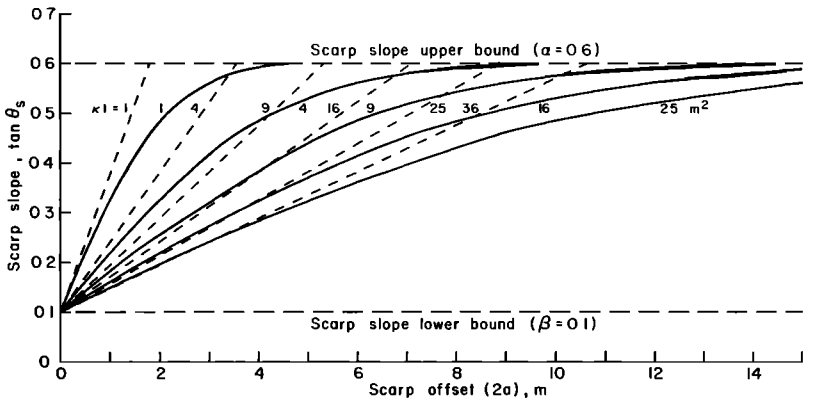

Fig. 12. Slope-offset relations for the vertical initial value scarp (dashed lines, equation (8)) and the finite slope, initial value scarp (solid curves, equation (21)), all lines and curves specified by the parameter κt (m^2). The choices of $\alpha = 0.6$ and $b = \beta = 0.1$ are nominally consistent with the Lake Bonneville shoreline slope-offset data (see Figures 11 and 13 and associated discussion in text).

The equivalent result for the initially vertical scarp is, again, equation (8);

$$\left.\frac{\partial u}{\partial x}\right|_{x=0} = \frac{a}{(\pi\kappa t)^{1/2}} + b$$

where $b = \beta$ = the far-field slope.

(Less obvious is how (21) reduces to (8) as the initial scarp slope tends to vertical, that is as $\alpha \rightarrow \infty$. This may be shown by recognizing that for finite a, the limit $\alpha \rightarrow \infty$ implies the limit $x_1 \rightarrow 0$, where x_1 is defined in equations (20). Substitute $x_1 = a/\alpha$ into (21) and expand it in a Taylor series about $x_1 = 0$ to obtain (8).)

Figure 12 compares evaluations of (21) and (8) for five choices of κt: 1, 4, 9, 16, and 25 m^2; (8) is also evaluated for 36 m^2. In all cases, $\alpha = 0.6$ and $\beta = 0.1$ were used in (21), values nominally consistent with the Lake Bonneville shore data to which we return shortly. At fixed κt the finite slope initial scarps always have smaller scarp slopes than the initially vertical scarps for $2a > 0$; the difference between them becomes progressively larger, at any fixed κt, for increasing offset $2a$. Physically, we may look at these differences in the following way: a large $2a$ scarp at fixed $\alpha < \infty$ appears much older than it is relative to the $\alpha = \infty$ calculation (8), because in the latter framework we think a lot has happened to $\partial u/\partial x|_{x=0}$, when in fact nothing has happened to it. In any event, the nonlinear form (21), which seems to be just what we need to interpret the Lake Bonneville shoreline slope offset data in Figure 11, arises purely as a matter of initial condition geometry, not as a matter of nonlinear modification processes.

The Lake Bonneville κ. In Figure 13, we plot the Lake Bonneville shoreline slope-offset data alone (solid circles of Figure 11); Figure 12 may be used as a template for Figure 13, and by inspection one infers κ between 9 and 25 m^2. In Figure 13, we present three evaluations of (21), to illustrate, in addition, the effect of variable α; we take $\beta = \tan\theta_f = 0.1$ to be well determined by the inset of Figure 11. The three calculations are for $\kappa t = 9$ m^2, $\alpha = 0.5$; $\kappa t = 16$ m^2, $\alpha = 0.6$; and $\kappa t = 25$ m^2, $\alpha = 0.7$. We consider the $\kappa t = 16$ m^2, $\alpha = 0.6$ curve to be the best overall fit to the data; thus we determine $\kappa = 1.1$ GKG for the Lake Bonneville shoreline scarps if we may assume, as this model requires, that the scarps were formed with initial slope angles of 31°, just somewhat less than the conventionally assumed $\theta_r = 35°$. Even so, we note that the $\kappa t = 9$ m^2, $\alpha = 0.5$ curve appears to be the slightly better fit for $2a \leq 4$ m and that the $\kappa t = 25$ m^2, $\alpha = 0.7$ curve appears to be the slightly better fit for $2a \geq 8$ m. Thus nonlinear modification processes may yet have contributed to the present morphology of the Lake Bonneville shoreline scarps. For the purposes of this investigation, however, we can safely neglect them. Any remaining uncertainties in the Lake Bonneville shoreline κ are surely no more than ±50% for a range in $2a$ that spans an order of magnitude. This uncertainty can be reduced even further if we can discount the $\kappa t = 9$ m^2, $\alpha = 0.5$ model as having an unreasonably low initial slope angle (26°). The Fish Springs Range fault scarps (Figure 15), for example, show no indication of having bounding scarp slopes at 0.5 (or for that matter at 0.6). While these are the youngest fault scarps we analyze in this study, they are, at an estimated age of 3000 years, hardly brand-new.

It is worthwhile noting that while the estimate here of $\kappa t = 16$ m^2 is 4 times less than that obtained (65 m^2) from the straight-line fit ($\alpha = \infty$) to the slope offset data (Figure 11, dashed line), it is much less discordant with the κt results from the profile modeling. For the smaller scarps ($2a < 2$ m), we also obtained $\kappa t = 16$ m^2, and the value for the intermediate scarps ($3.5 \leq 2a \leq 7$ m) is only nominally larger ($\kappa t = 25$ m^2). Only for the very largest scarps did the profile modeling yield a significantly larger κt (49 m^2). The bias in κt for the largest scarps is not surprising, since the $\kappa t = 16$ m^2 dashed-line model in Figure 12 reveals that any initially vertical Lake Bonneville shoreline scarp with $2a \gtrsim 7$ m "should" yet stand at $\theta_s \geq \theta_r$. What is surprising, in view of this geologically preposterous implication, is that scarps of this $2a$ and only somewhat smaller (Figure 8*a*) yield κt values (20–25 m^2) from the initially vertical scarp model that are only nominally biased (50% or less) with respect to that obtained from the finite slope, initial value calculations. It is for this reason that we believe that the κt value for Santa Cruz sea cliff A is not significantly biased, even though it "should" have spent 40% of its age at $\theta_s \geq \theta_r$ according to (8). The scarps in Figure 8*a*, for example, all "should" have spent a greater fraction of their age at $\theta_s \geq \theta_r$.

The age of the Drum Mountains fault scarps. Figure 14 is the slope-offset plot for all 49 profiles across the Drum Mountains fault scarps. The solid symbols indicate those profiles for which θ_f has a first significant digit of zero. Nor surprisingly, according to either (8) or (21) the scarp slopes for these profiles

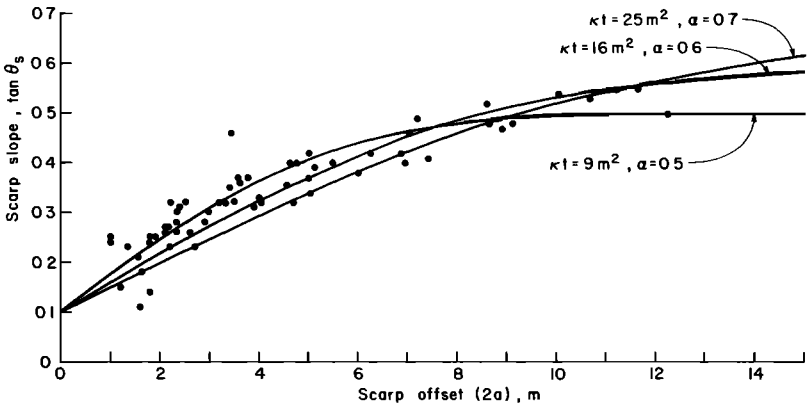

Fig. 13. The Lake Bonneville shoreline slope-offset data alone (solid circles of Figure 11), together with three evaluations of (21) to illustrate the effect of variable α. The preferred calculation is the $\kappa t = 16$ m^2, $\alpha = 0.6$ model, yielding $\kappa = 1.1$ GKG for the Lake Bonneville shoreline scarps.

always occupy the lower range of θ_s at any value of $2a$. A significant feature of the data is the sharp break in the trends of the data about the vertical line $2a \simeq 4$ m. For $2a < 4$ m, the straight-line fit (dashed line) seems reasonable, and from it we obtain $\kappa t = 5.8$ m^2 and $\theta_f = 2°$. The former is in good agreement with the profile modeling of the three smaller scarps (Figure 9), for which we obtained $\kappa t = 6.25$ m^2; the latter is in good agreement with the center of the distribution of fan slope angles (inset, Figure 14). With $\kappa t = 6$ m^2 for the smaller scarps we estimate their age to be 5.6 ka, using the Lake Bonneville κ of the last section.

The larger scarps are harder to deal with, but the negative curvature of the slope-offset data together with the very flat faces of the larger scarps ($2a = 5.0$ and 7.0 m, Figure 9) suggest the finite slope, initial scarp calculation (21). Two are presented in Figure 14, one for $\kappa t = 6.25$ m^2, $\alpha = 0.6$ and the other for $\kappa t = 4$ m^2, $\alpha = 0.5$. The latter is the better and a good fit to the data, but for this model we must rationalize the low initial scarp angles of 26°. The other model is not so good a fit to the data, but it gives us less problems rationalizing initial angles of 31°. In either case, however, all of the scarps are of the same age, 3600–5700 years if either value of κt is permissible. This is almost exactly the same result we obtained in the profile modeling section, although there it applied only to the smaller ($2a \lesssim 4$ m) scarps.

Yet another way of considering the slope-offset data for the Drum Mountains fault scarps is with the repeated faulting slope offset relation (14). Assuming the uplift rate A to be constant and setting $(2a)^{1/2} = (2At)^{1/2}$, we may write (14) as

$$\left.\frac{\partial u}{\partial x}\right|_{x=0} = \left(\frac{A}{\pi\kappa}\right)^{1/2} (2a)^{1/2} + 0.03 \qquad (22)$$

where initial value scarps have been neglected (set equal to zero) and $b = 0.03$ on the basis of the fan slope distribution (inset, Figure 14). However naive this continuous slip representation for a discrete faulting process (that need involve no more than two events), equation (22) says that the scarp slope should increase with $(2a)^{1/2}$, and this seems to be consonant with the observations. The dot-dashed curve in Figure 12 has been evaluated with $(A/\pi\kappa)^{1/2} = 0.175$ m$^{-1/2}$ which, for the Lake Bonneville κ, yields an uplift rate $A = 1.1 \times 10^{-4}$ m/yr. To form 6-m-high scarps at the rate $2A$ then requires 27 ka. This violates the geologic constraints by a factor of 2 in age.

Since the Lake Bonneville shoreline κ is unlikely to be uncertain to a factor of 2, the repeated faulting model does not seem likely. On the other hand, it is worth remembering that however certain we may regard the Lake Bonneville shoreline κ to be, this does not necessarily mean we can transfer it to the Drum Mountains fault scarps with comparable uncertainty. If, for some reason, the true Drum Mountains fault scarp κ is larger than the Lake Bonneville shoreline κ by only a factor of 2, multiple faulting for the larger Drum Mountains fault scarps remains a possibility (to the extent (22) fits the data). Nevertheless, it seems more likely that all the Drum Mountains fault scarps were formed in a single episode of normal faulting 3.6–5.7 ka B.P. Our preferred estimate is 5.6 ka, on the basis of $\kappa t = 6$ m^2 being valid for the profile modeling and the slope-offset representation for the smaller ($2a \lesssim 4$ m) scarps and our reluctance to accept $\alpha = 0.5$. Moreover, as

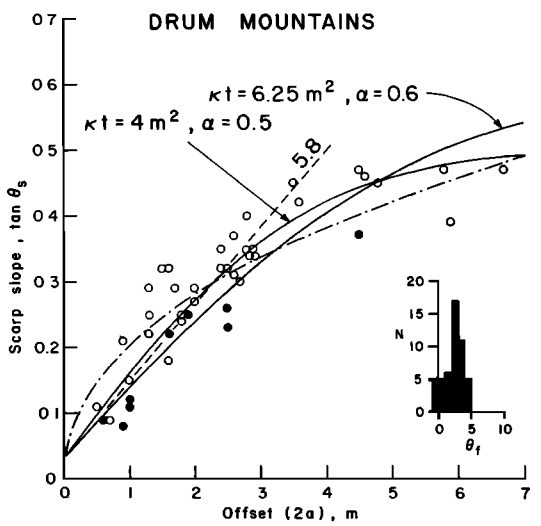

Fig. 14. Slope-offset plot for the Drum Mountains fault scarps. The smaller scarps ($2a < 4$ m) are well represented by the straight-line fit (dashed line), equation (8) with $\kappa t = 5.8$ m^2 and $b = 0.03$. The former is in good agreement with the results from profile modeling, and the latter is in good agreement with the median of the distribution of fan slope angles (inset). The two solid curves are an evaluation of (21) with the indicated parameters (and $\beta = 0.03$), and the dot-dashed curve is a repeated faulting model according to (22); all of these calculations are discussed at length in the text. The solid circles are slope-offset representations of profiles for which θ_f has a first significant figure of zero.

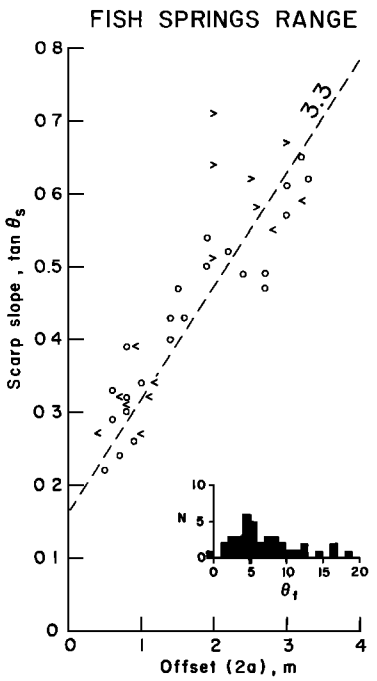

Fig. 15. Slope-offset plot for the Fish Springs Range fault scarps. "Greater than" symbols refer to slope-offset pairs with $\theta_f > 11°$, and the "less than" symbols refer to slope-offset pairs with $\theta_f < 4°$. The dashed-line fit yields $\kappa t = 3.3$ m^2 and $\theta_f = 9°$ (inset, as in Figures 11 and 14).

we shall see in the next section, the younger age estimate is nearly coincident with the age of the Fish Springs Range fault scarps, which morphologically appear to be distinctly younger than the Drum Mountains fault scarps.

Other fault scarps in west-central Utah. Figures 15, 16, and 17 are, respectively, the slope-offset plots for fault scarps of unknown age near the eastern base of the Fish Springs Range, 85 km northwest of Delta, Utah; along the western margin of the Oquirrh Mountains, southwest of Salt Lake City; and along the northeastern flank of the Sheeprock Mountains, 60 km north of Delta. All of these scarps cut weakly consolidated alluvial material similar to that cut by the Lake Bonneville shoreline. In all cases, the slope-offset data exhibit little if any curvature, in sharp contrast to the Lake Bonneville shoreline and Drum Mountains fault scarp data. In this section, then, we work exclusively with (8); the data themselves are reasonably well behaved with respect to straight-line model fits, and there is only one problem with intercept value mismatches, a problem that cannot be resolved with (21).

The Fish Springs Range data were considered by *Bucknam and Anderson* [1979], who noted that these scarps are younger than the Provo II level of Lake Bonneville. Both the freshness of the scarps themselves and their positioning with respect to the Lake Bonneville shoreline data on the scarp slope angle/scarp height plot suggested to *Bucknam and Anderson* [1979] that the most likely age of these fault scarps is "a few thousand years."

In Figure 15, the straight-line fit to the data yields $\kappa t = 3.3$ m^2 and $\theta_f = 9°$. The age of these scarps is then 3 ka, given that the Lake Bonneville shoreline $\kappa = 1.1$ GKG is appropriate. The estimated fan slope is only slightly greater than the average fan slope, the distribution of fan slopes being shown as the inset. Data from profiles with fan slopes greater than 11° are indicated by the "greater than" symbol, and data from profiles with slopes less than 4° are indicated by the "less than" symbol; generally, the former lie above the straight-line fit, and the latter lie below it, as expected. While this is by no means a one-to-one correlation, it does indicate that some of the "scatter" in such plots is a systematic effect of variable far-field slope.

The Oquirrh Mountains fault scarps are cut by the Lake Bonneville shoreline and thus are older than 14–15 ka B.P. In Figure 16, the straight-line fit is hardly well determined, and the data are limited in number; it yields $\kappa t = 35$ m^2 and $\theta_f = 5°$. The age of these scarps, again as fixed by the Lake Bonneville shoreline κ, is 32 ka, exclusive of the uncertainty in estimating the true slope of the observations. This age estimate meets the weak geologic constraint. The two points at $2a = 31.$ and 3.2 m possess the largest θ_f in the data set, 6.5° and 5.5°, respectively, and have not been given much consideration in the straight-line fit.

The final example is the Sheeprock Mountains fault scarps (Figure 17), for which there is no field control on age. The straight-line fit is remarkably good for the $2a \leq 7.2$ m data. The high point at $2a = 7.6$ m is associated with the largest fan slope, $\theta_f = 7.3$, and even the point at $2a = 11.5$ m is not far removed from the straight-line fit, although we have not given much consideration to either of these points with the straight-line fit. For this fit, $\kappa t = 58$ m^2 and $\theta_f = 4\frac{1}{2}°$. Again with the Lake Bonneville shoreline κ, we estimate the age of these scarps to be 53 ka. The intercept value, however, is about a factor of 2 higher than the center of the fan slope distribution (inset), which suggests that the straight-line fit, as good as it is, should not be taken too literally. The finite slope, initial value scarp model (21) will not help us here, since there is very little curvature in (21) at large κt and small $2a$ (Figure 12). An alternate interpretation, one hard to explore with the limited data, is that κt is somewhat smaller than 58 m^2 for the smaller ($2a \lesssim 5$ m) scarps, so to intercept a smaller θ_f, and that κt is somewhat larger than 58 m^2 for the larger ($2a \gtrsim 6$ m) scarps. Such adjustments need only be minor and would change the age estimate hardly at all. The principal argument for this possibility is that we are otherwise left with an 11.5-m offset occurring in a single event, faulting displacements ordinarily associated only with great earthquakes.

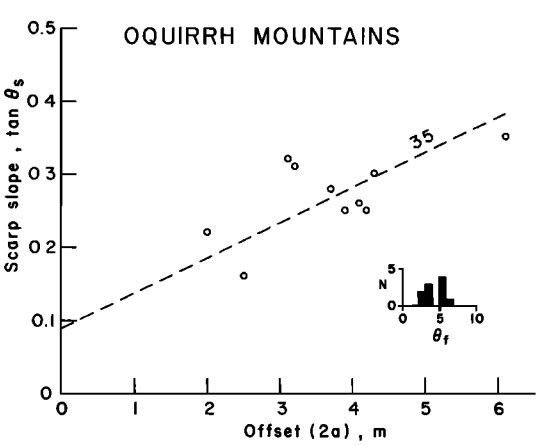

Fig. 16. Slope-offset plot for the Oquirrh Mountains fault scarps. The dashed-line fit yields $\kappa t = 35$ m^2 and $\theta_f = 5°$. The two points at $2a = 3.1$ and 3.2 m possess the largest θ_f in the data set (inset, as in Figures 11, 14, and 15).

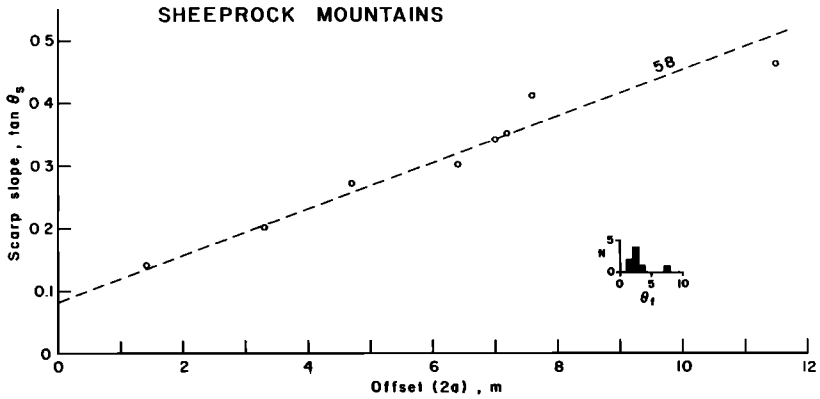

Fig. 17. Slope-offset plot for the Sheeprock Mountains fault scarps. The dashed-line fit yields $\kappa t = 58$ m^2 and $\theta_f = 4\frac{1}{2}°$. The point at $2a = 7.6$ m possesses the highest θ_f in the data set (inset, as in Figures 11, 14, 15, and 16). A two-event analysis (not shown), in which the smaller scarps ($2a \lesssim 5$ m) were slightly younger and the larger scarps ($2a \lesssim 5$ m) were slightly older would (1) decrease the intercept value to a more reasonable θ_f and (2) eliminate the conclusion that a 11.5-m offset occurred in a single earthquake (see text).

Discussion

This study has focussed more intensively on analytical equations, data representations, and interpretive problems than it has on specific results for the geologic structures considered herein. We have done so intentionally, in part because of the presently tentative nature of how this sort of landform analysis should proceed and in part because of the real advantages and disadvantages of the two data representations and their associated mathematical forms. In fact, the principal conclusions of this investigation, recounted in the next and final section, are related to these matters alone.

One purpose of this section, then, is to bring the individual numerical results, whether they be κ estimates or age determinations, together in a common context and, in the case of the Drum Mountains fault scarps, to compare them to the results of *Nash* [1980*b*]. It is worth reemphasizing the preliminary nature of the numerical results summarized below. The various geologic features we have examined have been considered largely in the context of illustrating a particular analytical form or a particular data representation (or both); each of these geologic features can and should be the subject of more thorough investigation, both observationally and analytically. Our numerical results for the Santa Cruz sea cliffs and the Raymond fault, for example, are particularly tentative, based as they are on single profiles. At the end of this section we bring together several observations concerning the use and misuse of slope-offset plots.

The κt Determinations

Table 2 summarizes the κt determinations of this investigation and the determination of κ/A for the Raymond fault; these determinations have been broken into separate entries for κ (GKG) and t (age in ka B.P.) or $2A$ (m/ka). The italicized quantities have been assumed known, thereby fixing the other quantity in any row. In addition, Table 2 includes two entries from the work of *Nash* [1980*a*] and one based on an observation of M. N. Machette (personal communication, 1982), that approximately meter-high, ~100 ka B.P. scarps are rare to nonexistent in alluvial terranes of the Basin and Range Province and of the Rio Grande Rift Valley as well.

In the case of the Santa Cruz sea cliffs, the inferred ages of sea cliffs A, B, and C have been used to determine a κ for each; more precisely, we simply used the same κ for each model fit and found that this worked. Of the three ages, that for sea cliff A is by far the best determined. It does not seem at all likely that sea cliff A can be less than 83 ka B.P. nor more than 125 ka B.P. The ages of sea cliffs B and C are only as good as the assumption of a uniform uplift rate for the past 400 ka. To return sensibily constant κ, however, it is only really necessary that sea cliff B be in the range of 200–300 ka B.P. and sea cliff C be in the range of 300–400 ka B.P.

With these "relaxed" ages the two significant figures for κ are misleading; more appropriately, they all may be considered as 10 GKG, but the important issue is that κ is approximately the same for these three structures, that is, over the past 400,000 years. Evidently, the known climatic variations in the recent past with periods of tens of thousands of years average out on time scales of a hundred or so thousand years.

Surprisingly, the κ estimate for the fan material cut by the Raymond fault is very much the same, 16 GKG, as for the Santa Cruz sea cliffs and represents a similar time span, 230 ka. Provided that both of these single-profile estimates are sustained by further investigations, we suspect that the higher rainfall in the Santa Cruz area is offsetting, at least in part, the more competent nature of the Santa Cruz Mudstone, in comparison with the precipitation and fan material in the vicinity of the Raymond fault.

By a factor of 15, the Lake Bonneville shoreline κ (1.1 GKG) is lower than that for the Raymond fault, although both structures are cut in weakly consolidated fan material. This difference must be mostly if not entirely due to climatic differences, presumably rainfall.

In addition to these three estimates of κ, Table 2 also includes two from *Nash* [1980*a*], who determined $\kappa = 12$ GKG from profile modeling of two sets of wave-cut bluffs in Emmet County, Michigan, one cut by glacial Lake Algonquin 730 ft (223 m) above sea level (abandoned 10.5 ka B.P.) and the other cut by Nipissing Great Lakes at 620 ft (189 m) above sea level (abandoned 4 ka B.P.). Both sets of bluffs are cut in predominantly sandy debris of glacial origin. This value of κ is similar to those determined here for the Santa Cruz sea cliffs and the Raymond fault, surprisingly so since the Emmet County value represents both unconsolidated material and a high level of precipitation. Vegetation cover, then, may be yet another variable for κ.

TABLE 2. Summary of Numerical Results

Geologic Structure	κt, m^2	κ/A, m	κ, GKG	t, ka B.P.	$2A$, m/ka
Santa Cruz sea cliffs					
A	1200		11	*105*	
B	2500		11	*230*	
C	4100		11	*370*	
Raymond fault		240	16	(230)*	*0.13*
Lake Bonneville shoreline	16		1.1	*14–15*	
Drum Mountains fault scarps†					
$\alpha = 0.5$	4		*1.1*	3.6	
$\alpha = 0.6$	6.25		*1.1*	5.7	
	6		*1.1*	5.6	
Fish Springs Range fault scarps	3.3		*1.1*	3	
Oquirrh Mountains fault scarps	35		*1.1*	32	
Sheeprock Mountains fault scarps	58		*1.1*	53	
Emmet County, Michigan, wave-cut bluffs					
Lake Algonquin	126		12	*10.5*	
Nipissing Great Lakes	48		12	*4*	
Machette constraint	≥ 100		≥ 1.0	*100*‡	

Italicized values are assumed known.

*Age estimate from $2At = 100$ ft = 30 m divided by $2A = 0.13$ m/ka.

†The last entry for these scarps ($\kappa t = 6$ m^2) is the average of the κt values determined from profile modeling and the slope-offset plot of the smaller ($2a \sim 4$ m) scarps alone.

‡The "unobservable" ($a = 1$ m) scarp of age 100,000 years: $\theta_s \leq 3° + \theta_f$.

Finally, the Machette constraint can be written in terms of the minimum observable scarp slope, which we take to be 3° above the fan slope on which such a scarp might be placed. Then

$$\tan (3° + \phi_f) \geq \frac{a}{(\pi\kappa t)^{1/2}} + b \qquad (23a)$$

or, for small θ_f,

$$0.052 \geq \frac{a}{(\pi\kappa t)^{1/2}} \qquad (23b)$$

That is, a 2-m-high scarp ($a = 1$ m) will be "observable," that is, have $\theta_s \geq 3° + \theta_f$, after 100,000 years only if $\kappa \leq 1.2$ GKG. That such scarps are not "observable" implies $\kappa \geq 1.2$ GKG. In Table 2 this entry is written as $\kappa \gtrsim 1$ GKG to reflect some uncertainty as to what is observable and what is not. The Lake Bonneville shoreline κ meets this constraint but just barely. Nevertheless, if our formulation of the Machette constraint (equations (23)) is at all close, the coincidence between the Machette inequality and the Lake Bonneville shoreline κ suggests that $\kappa \simeq 1$ GKG may be widely applicable to weakly consolidated alluvial terranes of the Basin and Range and Rio Grande Rift Valley, on time scales of both 14 and ~ 100 ka. Profiles of the Lake Lahontan shoreline scarps in western Nevada recently acquired by two of us (T.C.H. and R.E.W.) suggest this is indeed the case; when normalized for variable $2a$ and b, these profiles are indistinguishable from the Lake Bonneville shoreline scarps.

Table 2 also includes the four sets of fault scarps dated in this study on the basis of the Lake Bonneville shoreline κ. The Drum Mountains fault scarps have given us the most problems. The best model fit ($\kappa t = 4$ m^2, $\alpha = 0.5$, Figure 14) is the hardest for us to accept, in part because of the resulting young age (3.6 ka) and in part because of the low initial scarp angles (26°). We prefer the age estimate of 5.6 ka based on the smaller scarps alone ($\kappa t = 6$ m^2), even if this leaves us uncertain about the true significance of the larger scarps ($2a \gtrsim 4$ m). Consistent with their fresh-looking appearance, the Fish Springs Range fault scarps are very young; we estimate their age to be 3 ka. The age of the Oquirrh Mountains fault scarps, while more uncertain than the 32 ka entered in Table 2 because of the observations themselves (Figure 16), meets the weak constraint that these scarps are older than the Lake Bonneville shoreline. The Sheeprock Mountains fault scarps are even older, 53 ka. They are remarkably well grouped with respect to a straight-line fit, but our inability to recover the average θ_f (by a factor 2) suggests that this appearance may be illusory. Our age estimate would not be much affected, however, by a two-event analysis that would better match the intercept value.

Nash [1980*b*] has also analyzed the Drum Mountains fault scarps data, as presented in the scarp slope angle/scarp height representation of *Bucknam and Anderson* [1979]. Assuming that all faults were formed 10,000 years ago on faults dipping at 25°, *Nash* [1980*b*] determines that $\kappa = 4.4 \times 10^{-4}$ m^2/yr. The calculations were performed numerically, but his estimate of $\kappa t = 4.4$ m^2 (given $\alpha = 0.47$) is remarkably close to the $\kappa t = 4$ m^2, $\alpha = 0.5$ model in Figure 14. *Nash* [1980*b*] then reversed what we have done here, namely determining κ from an assumed age. Both in *Nash's* [1980*b*] study and this one, however, the problem is to rationalize $\alpha = 0.5$. Typical values of normal fault dips in the Basin and Range are in the neighborhood of 60°; a single trench exposure of one Drum Mountains fault scarp reveals a fault dip of 76° [*Crone*, 1983]. Initial scarp angles of 25° are even significantly less than $\theta_r \simeq 35°$. A consequence, then, of both these $\kappa t \simeq 4$ m^2, $\alpha \simeq 0.5$ models is that, in the absence of nonlinear modification processes, the larger scarps are essentially unchanged from the day they were "formed," since the calculations yield scarp slopes at $2a > 4$ m only incrementally changed from the initial value of 25° or 26° [*Nash*, 1980*b*, Figure 3] (Figure 14 of this study).

The Slope-Offset Plots

Consistent with the diffusion equation analysis that is the basis of this study, we have restructured the scarp slope angle/scarp height diagram of *Bucknam and Anderson* [1979] into the slope-offset plots used extensively in this study. With-

out losing any of the observational advantages of the scarp slope angle/scarp height diagrams to accommodate large sets of point pairs, the slope-offset representation permits quantitative analysis to be performed directly in the data space. It moreover makes use of the intercept value b at $2a = 0$; any model fit, diffusion equation mathematics or otherwise, must meet this constraint which comes essentially for free. Indeed, failure to meet this constraint can be taken as almost a sure sign of real or impending difficulties. Finally, the slope-offset plots allow for the systematic effects of variable b. While variable far-field slopes are hardly responsible for all of the scatter in slope-offset plots, they are surely contributing some of it (Figures 13–17).

Relative to profile modeling, slope-offset analysis also has several advantages. Profile modeling is not only time and space consuming, but the appropriate mathematical forms are more cumbersome to use. Nevertheless, modeling of even a few profiles can illuminate a $\kappa t - 2a$ dependence that otherwise might be hard to see (or easy to ignore) in the slope-offset plot. Moreover, profile modeling permits an assessment of model fit to data in the cross-strike direction (where the effects of multiple scarps may be found, for example) that the slope-offset representation does not see. As such, slope-offset analysis should not, in general, stand apart from modeling of at least a few profiles that span the range of $2a$.

SUMMARY AND CONCLUSIONS

The principal purpose of this study has been to apply analytical equations, within the restrictions of the diffusion equation model, to real observations of wave-cut and faulting-controlled landforms, as these landforms have been modified across arbitrary and generally unknown periods of time. In broad outline, its principal conclusion is that this diffusion equation representation, even in its most elementary model solutions, makes sense, within limits, for the wide class of observations considered here ($1 \lesssim 2a \lesssim 50$ m, $3 \lesssim$ age $\lesssim 400$ ka B.P.).

Numerically, the results of this study are summarized in Table 2, as qualified by the caveats of the preceding discussion section. In broader terms, we see the following as the principal conclusions of this study. Model solutions of the most elementary type to the diffusion equation can reproduce the actual topography of scarplike landforms with remarkable accuracy. There seems little doubt, then, that diffusionlike processes contribute significantly to the modification of nondissecting alluvial terranes, even if the constant coefficient, homogenous diffusion equation does not incorporate each and every one of them. Significantly, most although not all of the observations that could be interpreted as evidence for nonlinear modification processes, namely, the $\kappa t - 2a$ dependences for the Lake Bonneville shoreline and Drum Mountains fault scarps, are as easily attributed to the effect of finite slope, initial value scarps. The price of this interpretation comes in the form of the two unanswered questions of this study, both associated with the Drum Mountains fault scarps: why are these fault scarps the only set of four to show evidence for bounding scarp angles and why are these bounding scarp angles so small? The most intriguing result of this study is the coincidence between the Lake Bonneville shoreline κ (1.1 GKG) and the κ ($\gtrsim$1 GKG) derived from the Machette constraint. If this coincidence is physically significant, it means that the Lake Bonneville shoreline κ is widely applicable to unconsolidated alluvial terranes throughout the Basin and Range and Rio Grande Rift Valley, on time scales of 10-100 ka. In any event we have used this κ to date four sets of fault scarps in west-central Utah. The age estimates meet available geological constraints, although we are yet uncertain about the true significance and age of the $2a \gtrsim 4$ m Drum Mountains fault scarps.

All of this is sufficient to suggest, at least to us, that the diffusion equation representation, when used within sensible limits, holds considerable promise as an analytical model of the evolution of wave-cut and faulting-controlled landforms in terranes degradable on time scales of hundreds of thousands of years or less. Practically speaking, this approach seems very promising as a means of dating fault scarps of unknown age with observations that are extraordinarily easy to come by. Age estimates, however, will only be as accurate as the κ borrowed from some other structure of known age. Extracting this κ in the first place is not without nuance and uncertainty; transferring it to another area and structure involves entirely different uncertainties, of which not much is known. If research such as this is to progress much further, then, it will be through a collection of well-defined κ estimates, so we may more clearly understand how κ varies as a function of material, climate, vegetative cover, and, of course, time.

Acknowledgments. The observation without which this study would not be was made on a fault trip skillfully organized by J. B. Rundle in December 1981. D. D. Pollard pointed us to the transcription of G. K. Gilbert's field notes (A. M. Johnson and D. D. Pollard, unpublished manuscript, 1977), and he and P. Segall saw through the trigonometry of equation (11). A. J. Crone gave us a guided tour of his trench excavation on the Drum Mountains fault scarps in May 1982. M. N. Machette arranged an opportunity for T.C.H. and R.C.B. to discuss these matters at the U.S. Geological Survey, Golden, Colorado, with S. M. Colman, A. J. Crone, L. Mayer, M. N. Machette, A. R. Nelson, K. L. Pierce, and D. P. Russ, who scrutinized our ideas at an early date (July 14, 1982). The critical commentary of A. H. Lachenbruch, W. Thatcher, and M. L. Zoback have been of great help in getting our ideas to their present form. Lachenbruch suggested to us the finite slope, initial value problem at a time when we were prepared to attribute the $\kappa t - 2a$ dependence for the Lake Bonneville shoreline scarps solely to nonlinear modification effects. We have utilized the commentary of W. B. Bull, L. Mayer, D. B. Nash, and R. P. Sharp in preparing the printed version. Ray Eis carefully constructed the illustrations from originals bordering on the unintelligible, and Carol Sullivan patiently typed this manuscript several times with unfailing accuracy. One of us (T.C.H.) has enjoyed the support of a G. K. Gilbert fellowship of the U.S. Geological Survey during the course of this study.

REFERENCES

Bloom, A. L., W. S. Broecker, J. M. A. Chappell, R. K. Matthews, and K. J. Mesolella, Quaternary sea level fluctuations on a tectonic coast: New $^{230}Th/^{234}U$ dates from the Huon Peninsula, New Guinea, *Quat. Res.*, *4*, 185–205, 1974.

Bradley, W. C., and W. O. Addicott, Age of first marine terrace near Santa Cruz, California, *Geol. Soc. Am. Bull.*, *79*, 1203–1210, 1968.

Bradley, W. C., and G. B. Griggs, Form, genesis, and deformation of central California wave-cut platforms, *Geol. Soc. Am. Bull.*, *87*, 433–449, 1976.

Bucknam, R. C., and R. E. Anderson, Estimation of fault-scarp ages from a scarp-height-slope-angle relationship, *Geology*, *7*, 11–14, 1979.

Carslaw, H. S., and J. C. Jaegar, *Conduction of Heat in Solids*, 510 pp., Oxford University Press, New York, 1959.

Clark, M. M., A. Grantz, and M. Rubin, Holocene activity of the Coyote Creek fault as recorded in sediments of Lake Cahuilla, *U.S. Geol. Surv. Prof. Pap.*, *787*, 112–130, 1972.

Crone, A. J., Amount of displacement and estimated age of a Holocene age surface faulting event, Eastern Great Basin, Millard County, Utah, *Spec. Stud. Utah Geol. Miner. Surv.*, *62*, 49–55, 1983.

Crook, R., Jr., C. R. Allen, B. Kamb, C. M. Payne, and R. J. Proctor, Quaternary geology and seismic hazard of the Sierra Madre and

associated faults, western San Gabriel Mountains, California, *U.S. Geol. Surv. Prof. Pap.*, in press, 1983.
Culling, W. E. H., Analytical theory of erosion, *J. Geol.*, *68*, 336–344, 1960.
Culling, W. E. H., Soil creep and the development of hillside slopes, *J. Geol.*, *71*, 127–161, 1963.
Culling, W. E. H., Theory of erosion on soil-covered slopes, *J. Geol.*, *73*, 230–254, 1965.
Gilbert, G. K., Lake Bonneville, *Monogr. 1*, 438 pp., U.S. Geological Survey, Reston, Va., 1890.
Hirano, M., A mathematical model of slope development—An approach to the analytical theory of erosional topography, *J. Geosci. Osaka City Univ.*, *11*, 13–52, 1968.
Hirano, M., Slope form and upheaval of the Yoro Mountain range, Central Japan (in Japanese), *Geol. Soc. Jpn. J.*, *75*, 615–627, 1969.
Kennedy, G. L., K. R. Lajoie, and J. F. Wehmiller, Aminostratigraphy and faunal correlations of late Quaternary marine terraces, Pacific Coast, USA, *Nature*, *299*, 545–547, 1982.
Machette, M. N., Quaternary and Pliocene faults in the La Jencia and southern part of the Albuquerque-Belen basins, New Mexico: Evidence of fault history from fault-scarp morphology and Quaternary geology, *Field Conf. Guideb. N. M. Geol. Soc.*, *33*, 161–170, 1982.
Mayer, L., Quantitative tectonic geomorphology with applications to neotectonics of northwestern Arizona, Ph.D. thesis, 213 pp., Univ. of Ariz., Tucson, 1982.
Nash, D. B., Forms of bluffs degraded for different lengths of time in Emmet County, Michigan, U.S.A., *Earth Surf. Processes*, *5*, 331–345, 1980*a*.
Nash, D. B., Morphologic dating of degraded normal fault scarps, *J. Geol.*, *88*, 353–360, 1980*b*.
Schumm, S. A., Rate of surficial rock creep on hillslopes in western Colorado, *Science*, *155*, 560–562, 1967.
Scott, W. E., R. R. Shroba, and W. D. McCoy, Guidebook for the 1982 friends of the Pleistocene, Rocky Mountain cell, field trip to Little Valley and Jordan Valley, Utah, *U.S. Geol. Surv. Open File Rep.*, *82-845*, 1–13, 1982.
Sieh, K. E., Prehistoric large earthquakes produced by slip on the San Andreas fault at Pallett Creek, California, *J. Geophys. Res.*, *83*, 3907–3939, 1978.
Soderblom, L. A., A model for small-impact erosion applied to the lunar surface, *J. Geophys. Res.*, *75*, 2655–2661, 1970.
Wallace, R. E., Profiles and ages of young fault scarps, north-central Nevada, *Geol. Soc. Am. Bull.*, *88*, 1267–1281, 1977.

R. C. Bucknam, U.S. Geological Survey, Denver Federal Center, Denver CO 80225.
T. C. Hanks, K. R. Lajoie, and R. E. Wallace, 345 Middlefield Road, Menlo Park, CA 94025.

(Received April 18, 1983;
revised November 29, 1983;
accepted January 17, 1984.)